ISTANBUL TECHNICAL UNIVERSITY ★ ENERGY INSTITUTE

NUMERICAL INVESTIGATION OF DIMENSIONAL INFLUENCES FOR PRESSURE DROP AND HEAT TRANSFER AUGMENTATION IN MICROCHANNELS

M.Sc. THESIS

Doğukan ARSLAN

Energy Science and Technology Division

Energy Science and Technology Programme

JUNE 2019

ISTANBUL TECHNICAL UNIVERSITY ★ ENERGY INSTITUTE

NUMERICAL INVESTIGATION OF DIMENSIONAL INFLUENCES FOR PRESSURE DROP AND HEAT TRANSFER AUGMENTATION IN MICROCHANNELS

M.Sc. THESIS

Doğukan ARSLAN
(301151041)

Energy Science and Technology Division

Energy Science and Technology Programme

Thesis Advisor: Prof. Dr. Filiz BAYTAŞ

JUNE 2019

İSTANBUL TEKNİK ÜNİVERSİTESİ ★ ENERJİ ENSTİTÜSÜ

MİKROKANALLARDA BOYUTSAL ETKİLERİN, ISI TRANSFERİ ARTIRIMINA VE BASINÇ DÜŞÜŞÜNE OLAN ETKİSİNİN SAYISAL İNCELENMESİ

YÜKSEK LİSANS TEZİ

Doğukan ARSLAN
(301151041)

Enerji Bilim ve Teknoloji Anabilim Dalı

Enerji Bilim ve Teknoloji Programı

Tez Danışmanı: Prof. Dr. Filiz BAYTAŞ

HAZİRAN 2019

Doğukan Arslan, a M.Sc. student of ITU Institute of Energy 301151041, successfully defended the thesis entitled “NUMERICAL INVESTIGATION OF DIMENSIONAL INFLUENCES FOR PRESSURE DROP AND HEAT TRANSFER AUGMENTATION IN MICROCHANNELS”, which he prepared after fulfilling the requirements specified in the associated legislations, before the jury whose signatures are below.

Thesis Advisor :	**Prof. Dr. Filiz BAYTAŞ** Istanbul Technical University	.....
Co-advisor :	**Assoc. Prof.Dr. Mustafa Fazıl SERİNCAN** Gebze Technical University	.....
Jury Members :	**Prof. Dr. Üner ÇOLAK** Istanbul Technical University	.....
	Prof. Dr. Hakan DEMİR Yıldız Technical University	.....
	Assist. Prof. Dr. Duygu ERDEM Istanbul Technical University	.....

Date of Submission : 02 May 2019
Date of Defense : 13 June 2019

To whole forgotten good people,

FOREWORD

First of all, I am frankly grateful to my supervisor who is Prof. Dr. Filiz BAYTAS and my co-advisor who is Assoc. Prof. Dr. Mustafa Fazıl SERINCAN. They supported me from beginning to end of my master thesis. I have possessed a quality academic study with their supervisions. Also, I want to thank my colleagues which are working in Gebze Technical University.
Finally, the greater appreciation belongs to my loved family who have been supporting me in my education life since I was in nursery school.

May 2019

Doğukan ARSLAN
(Mechanical Engineer)

TABLE OF CONTENTS

Page

ABBREVIATIONS

App	**:** Appendix
Geo	**:** Geometric structure
Kn	**:** Knudsen Number
MEMS	**:** Micro Electro Mechanical System
Nu	**:** Nusselt Number
NS	**:** Navier-Stokes
Pr	**:** Prandtl Number
PEC	**:** Performance evaluation criteria
Re	**:** Reynolds Number

LIST OF TABLES

Page

LIST OF FIGURES

Page

SYMBOLS

a	**:** Height of a flow channel
A_f	**:** Contact area between fluid and wall surface
b	**:** Wide of a flow channel
c	**:** Length of straight region in all models except straight channel
c_p	**:** Specific heat
d	**:** Length of modificated region in all models
D	**:** Smallest channel dimension
D_h	**:** Hydraulic diameter
e	**:** Relative error
f	**:** Fanning friction factor
f_o	**:** Fanning friction factor of a straight channel
f_o^*	**:** Corrected Fanning friction factor of a straight channel
H	**:** Characteristic length of channel
h	**:** Heat transfer coefficient
h_{avg}	**:** Average heat transfer coefficient
k	**:** Thermal conductivity
k_f	**:** Thermal conductivity of fluid
k_s	**:** Thermal conductivity of solid
L	**:** Length of microchannel
L_h	**:** Hyradulic entrance length
$\dot{m}$	**:** Mass flow
m_n	**:** Edge mesh parameters (n ϵ 1,2,3,4,5 and 6)
Nu_o	**:** Nusselt Number of a straight channel
Nu_o^*	**:** Corrected Nusselt Number of a straight channel
p	**:** Pressure
P_e	**:** Pressure drop of model which has coarser mesh type
P_o	**:** Pressure drop of model which has more fine mesh type
Pr_m	**:** Prandtl Number of a model
Pr_o	**:** Prandtl Number of a straight channel
$\dot{q}$	**:** Reynolds Number
Re_m	**:** Reynolds Number of a model
Re_o	**:** Reynolds Number of a straight channel
T	**:** Temperature
$T_{f,ave}$	**:** Average fluid temperature
T_s	**:** Solid temperature
T_i	**:** Inlet temperature
T_e	**:** Exit temperature
T_1	**:** Differences between inlet and exit temperature
T_2	**:** Differences between average wall and average fluid temperature
$T_{w,ave}$	**:** Average wall temperature
T_e	**:** Exit temperature

$\mathbf{u_{in}}$: Inlet velocity
$\mathbf{u_m}$: Mean velocity
$\mathbf{V}$: Velocity
$\mathbf{x}$: Distance from beginning
$\mathbf{x^+}$: Inverse of Greatz Number
$\boldsymbol{\rho_f}$: Fluid density
$\boldsymbol{\mu}$: Dynamic viscosity
$\boldsymbol{\mu_f}$: Fluid viscosity
$\boldsymbol{\mu_{in}}$: Fluid viscosity at inlet temperature
$\boldsymbol{\tau_w}$: Wall shear stress
$\boldsymbol{\lambda}$: Mean free path

NUMERICAL INVESTIGATION OF DIMENSIONAL INFLUENCES FOR PRESSURE DROP AND HEAT TRANSFER AUGMENTATION IN MICROCHANNELS

SUMMARY

Recently, with the development of technology, the size of the devices has been shrinked. One the best examples of this situation is the minimizing of computers and hardware components. With the shrinkage of parts, the problem of overheating becomes an even more serious problem because of local hot spots on devices. One of the many methods that can overcome this problem is microchannel.

In this thesis, in order to obtain influences of geometric modifications on heat transfer enhancement and fanning friction factor in microchannels, particular models are investigated numerically by using many different cases. There are 5 main models. Also, each model includes 9 sub-cases and diverse wall structures. Walls have a special sinusoidal function.

In order to draw sub-cases of the numerical investigation, Solidworks program was used. Also, ANSYS Design Modeler and Mesh programs were used in order to prepare sub-cases for analyses. ANSYS Fluent CFD was used for solving momentum, continuity and energy equations. SIMPLEC algorithm was used with second order discretization. Furthermore, the residuals are selected 10^{-4} for continuity and momentum equations also chosen 10^{-7} for energy equations.

Different influences were investigated in various designed 5 models. Shortly, Model 1 has only the reentrant cavities, therefore boundary layer interruption is targeted phenomena. Because of the reentrant cavities, sudden expansions occur and velocity gradients dramatically reduce, so values of wall shear which is related to fanning friction decrease significantly. In spite of Model 1, there are not only cavities but also ribs in Model 2. By virtue of these structures, sudden expansion and contraction ensue therefore increment in pressure drop and fanning friction factor are expected. Model 3 has wavy wall structure also cross-section is constant along the channel. In this model, the reentrant cavities and ribs are arranged in sync. Unlike Model 1, the reentrant cavities are collocated unsymmetrically in Model 4. Finally, Model 5 has only the reentrant ribs which are arranged unsymmetrically. Therefore, these ribs behave in the flow area as obstacles which increase fanning friction factor.

Throughout the master thesis, a special code was used in order to categorize sub-cases and increase comprehensibility. Each model is symbolized as M1, M2, M3, M4 and M5. Besides, there are 3 different sinusoidal function which have 3 various frequencies, so these functions are denoted as F1, F2 and F3. Moreover, in order to indicate 3 diverse aspect ratios, AR1/3, AR1 and AR3 were used. For example, when

M2_F3_AR1 is declared, that the sub-case has features of Model 2, third function and aspect ratio which is 1 must be understood.

Before starting analyses of models, with using M2_F3_AR1, mesh independence study was conducted in order to find optimum mesh structure. After solutions, Nusselt number and friction factor were calculated in order to compare the straight ones. Nusselt number depends on Pr, Re and geometric structure, therefore in order to find influences of geometric structure , correction coefficient which include Pr and Re, was applied to straight channels. This operation was made for friction factor because friction factor is related to Re. After all, Nu/Nu_o^* and f/f_o^* were gained with PEC number. However, in order that Nu values are valid, x^+ values must be calculated and known. Because, Nu value is related to thermal-entry length and when x^+ is calculated as 1, Nusselt Number which is calculated gives developed value at thermally fully developed flow.

In the results section, with using vertical and central horizontal planes were taken from sub-cases. existence of recirculation zones was noticed while frequency were high such as F3. Also, longitudinal and dean vortices were found in vertical planes. To sum up, M2_F2_AR1 was found as the best channel from among.

MİKROKANALLARDA BOYUTSAL ETKİLERİN, ISI TRANSFERİ ARTIRIMINA VE BASINÇ DÜŞÜŞÜNE OLAN ETKİLERİNİN SAYISAL İNCELENMESİ

ÖZET

Son zamanlarda, teknolojinin gelişmesiyle birlikte, elektronik cihazların boyutlarında küçülmeler olmuştur. İnsanların sosyal hayat ve iş yaşamında kullandığı cihazların, kompakt hale getirilmesine dair çalışmalar her zaman temel uğraş konularından biridir. Bu durumun en güzel örneklerinden birisi de bilgisayalar ve donanım parçalarının boyutlarının düşürülmesidir. Parçaların küçültülmesiyle birlikte, cihazlardaki bölgesel sıcak noktalar ile aşırı ısınma olayı daha da ciddi bir problem haline gelmiştir. Bu problemin üstesinden gelmek için kullanılabilecek yöntemlerden birisi mikrokanallardır.

Bu tez çalışmasında, ısı transferinin iyileştirilmesi ile basınç düşüşü arasında denge kurabilen bir model geliştirmek amacı ile geometrik değişikliklerin oluşturulduğu 45 alt model tasarlanmıştır ve sayısal analizler, sonlu hacimler metodu kullanan ANSYS Fluent CFD programı ile gerçekleştirilmiştir. Bu modellerin hepsi aynı alanı soğutacak şekilde tasarlanmıştır, böylece tüm modellerde sabit taban alanı mevcuttur. Beş temel model her biri dokuz alt modele sahip olacak şekilde gruplandırılmıştır.

Tez çalışmasında, oluşturulan modeller için analizlere başlamadan önce, literatürde seçilmiş bir çalışmanın belli değerleri ile doğrulama gerçekleştirilmiştir. Basınç düşüşü ve sıcaklık dağılımının karşılaştırıldığı bu doğrulama çalışmasında, dört farklı ağ yapısı kullanılarak optimum ağ yapısı oluşturulmuştur.

Matematik model olarak konjugat bir kanal seçilip hem ısı iletimi hem ısı transferinin etkileri dikkate alınmıştır. Sadece tabandan 20 W/cm^2 ısı akısı verilerek diğer duvar yüzeylerinde ısı yalıtımı olduğu kabulü yapılmıştır. Her alt modelin kanal yapısının ilk 7 mm'si düz olup, burada akışın hidrolik olarak gelişmesi istenmiştir. Kanalların 7 mm ile 9.513 mm'si arasında değişiklikler yapılmış ve bu bölge için özel bir hacim oluşturulmuştur. Hesaplamalar yalnızca bu hacim içinde yapılıp düz kanal etkilerinden arındırılmaya çalışılmıştır. Fluent analiz paketinde, algoritma olarak SIMPLEC seçilmiş ve diferansiyel denklemler ikinci dereceden çözdürülmüştür. Analizde, artık değerler (residuals), süreklilik, x, y ve z yönünde momentum denklemleri çözümü için 10^{-4} ancak enerji denklemleri için 10^{-7} olarak seçilmiştir. Bu değerler literatürde yapılan akademik çalışmalar göz önüne alınarak hassasiyeti artırmak için düşük seçilmiştir.

Tasarlanmış 5 farklı modelde, farklı etkiler araştırılmıştır. Model 1, içinde yalnızca oyukların bulunduğu ve sınır tabakanın kesintiye uğratılması hedeflenen bir yapıdır. Bu yapıda ani genişlemeler belirli bölgelerde hız gradyenlerin dikkate değer şekilde düşmesine sebep olmakta ve Reynolds sayılarını düşürmektedir. Model 2, hem oyukların hem de çıkıntıların (rib) olduğu daralmanın ve genişlemenin gözlemlendiği bununla birlikte yüksek basınç düşüşlerinin olduğu, sürtünme faktörünün yüksek çıkması beklenen bir modeldir. Model 3, dalgalı (wavy) kanal olarak literatürde yer bulan, akışın enine kesitinin sabit olduğu aynı anda hem oyuğun hem çıkıntının olduğu bir yapıya sahiptir. Model 4, Model 1'e benzemekte olup simetrik olmayan

oyuklara sahip bir kanal modelidir. Son olarak Model 5, Model 4'ün tam tersi olup simetrik olmayan oyuklar yerine yine simetrik olmayan çıkıntılar bulundurmaktadır.

Tez boyunca bir kodlama sistemi oluşturulmuştur. Her bir model M1, M2, M3, M4 ve M5 koduyla gösterilmiştir. Bunun yanı sıra her bir modelin alt modelini oluşturmak için 3 farklı frekansa sahip sinüs fonksiyonları kullanılmıştır. Bunlarda F1, F2 ve F3 olarak gösterilmiştir. Bir diğer farklılık olarak oluşturulan farklı en-boy oranları için AR1/3, AR1 ve AR3 olarak gösterim yapılmıştır. Yani M2_F1_AR1 dendiğinde, 2. modelin 1 numaralı fonksiyonuna sahip en-boy oranı 1 olan bir alt model anlaşılmalıdır.

Yukarıda anlatılan bütün modellerin alt modelleri Solidworks 2018 programında çizilip tasarlanmış ve daha sonra analize uygun hale getirmek için ANSYS Design Modeler programında çalışmalar yapılmıştır. Analizlere başlamadan önce uygun matematiksel ağ yapısının (mesh) seçilebilmesi için ağ atılması en zor olabilecek model olan M2_F3_AR1 modeli seçilerek beş farklı ağ yapısı uygulanmıştır. Bu çalışmada kullanlan farklı ağ yapıları kullanılan modellerin analizi yapılıp basınç düşüşleri incelenmiştir. En ince ağ yapısına sahip modele, en yakın hata oranında olan ve hız açısından daha hızlı olan optimum olduğu düşünülen ağ yapısı (Mesh 2) seçilmiştir.
Seçilen bu ağ yapısı bütün alt modellere uygulanarak 45 alt model analize uygun hale getirilmiştir. Bununla beraber 3 farklı en-boy oranına sahip düz kanallar da aynı ağ yapısıyla analiz edilmiştir.

Bütün alt modeller ve düz kanallar için seçilmiş hacimde Nusselt sayıları ve sürtünme faktörleri hesaplanmıştır. Ancak bu sonuçlar doğrudan kıyaslamak için uygun değildir. Çünkü düz ile değişime uğramış aynı en-boy oranına sahip kanalların Prandtl ve Reynolds sayıları aynı değildir. Bilindiği üzere Nusselt sayısı Pr, Re ve geometrik yapının bir fonksiyonudur. Sadece geometrik yapının etkisini görmek için düz kanalların her birisi için düzeltme faktörü kullanılmalıdır. Bu durum Re sayısına bağlı olan sürtünme faktörü içinde geçerlidir.

Her alt model, kendi en-boy oranına sahip düz kanalla kıyaslanarak Nu/Nu_o^* , f/f_o^* ve PEC değerleri bulunur. PEC değeri içerisinde hem Nusselt oranını hem de sürtünme faktörü oranını içerdiği için optimum kanalı bulmamızda bir performans değerlendirme göstergesidir. Unutulmamalıdır ki, hesaplanan Nu değerleri tek başlarına yeterli bir gösterge değildir. x^+ değerleri de bilinmelidir. Bu yüzden bütün kanallarda 7. mm de x^+ değerleri hesaplanmış olup, termal açıdan tam gelişmişliğe olan uzaklık belirtilmiştir.

Analizler sonunda, seçilen alt modellerde yatay ve dikey kesitler alınarak akış karakteristiği araştırılmıştır. Yatay kesitlerde en çok karşılaşılan problem devirdaim (recirculation) alanlarıdır. Bu bölgelerde akış çok yavaş hatta durma noktasına gelmektedir. Akışın bu denli yavaş olması taşınımla ısı transferinin düşmesine sebep olmaktadır, bu durumun Nusselt sayısını etkilediği görülmektedir. Alınan dikey kesitlerde eksenel girdaplar ve Dean girdapları bazı yapılarda karşımıza çıkmaktadır. En boy oranı düştükçe Dean girdapları daha belirgin hale gelmektedir. Bu belirtilen girdaplar akışta bir karıştırıcılık görevini üstlenmekte ve sıcak ile soğuk akışkanı birbirine karıştırmaktadır.

Sonuçlara bakıldığında, Nusselt sayısının yüksek çıktığı alt modellerde aynı zamanda sürtünme faktörlerinin de yüksek çıkması sebebiyle PEC değerlerinin düştüğü gözlenmektedir. Bu durum ısı transferi açısından iyileştirmenin sağlandığını ancak sürtünme faktörünün artmasıyla maliyeti artıran bir yöntem olduğunu göstermektedir. M2_F2_AR1 modelinin hesaplanan PEC değeri 1.18'dir ve diğer kanallarınkinden yüksektir. Bu yüzden M2_F2_AR1 modelinin %18 iyileştirmeye olanak sağlamasından dolayı bu problemde kullanılması tavsiye edilmektedir.

1. INTRODUCTION

The evolution of the technologies carries with the increasing request for great performance in electronic devices which encompass our business and daily life. This situation conduces toward a consequential question which is how to control thermal management in order to eliminate high heat dissipation and hot spots which are occurred in electronic devices. Especially, minimizing the package of the electronic devices sparks off more heat production per unit volume.

Cooling methods are applied in this circumstances in order to prevent permanent damages which arise due to exceeding heat generation. There are many methods such as conventional heat sinks, heat pipe, phase-change materials and thermoelectric coolers and microchannel cooling which will be discussed in this thesis study. In order to provide efficient protection for electronic appliances, the coolant must be selected as an appropriate refrigerant fluid. Mostly, air, water and refrigerants are selected fluids in microchannels. Air has been chosen coolant in microchannels in order to chill electronic appliances. Nevertheless, air chilling techniques have transformed into in sufficient for most implementations with heat fluxes cutting across 100 W/m^2. Liquid coolants, acquiring greater heat transfer coefficient than gaseous coolants, supply superior performance in chilling. Also, fluids which have greater specific heats and superior convection heat transfer coefficients are more effective in order to removing heat dissipation from boundaries (Tullius, Vajtai, & Bayazitoglu, 2011).

First microchannel cooling was illustrated by Tuckerman and Pease (Tuckerman & Pease, 1981) with the occasion of that high heat flux remotion capacity of equal to 790 W/cm^2 carried out. That increment in the heat transfer coefficient depends on decrement in the hydraulic diameter of channel was indicated by them.

In this thesis study, various investigations handling basic apprehension of microchannel structure and heat transfer enhancement methods such as figure of microchannels, modifications in cross-sections, ribs, cavities and fin structures are

shown. In the next sections, numerical investigation in microchannels which have various geometric structure combining with different aspect ratios and surface functions are displayed.

1.1 Purpose of Thesis

In this study, in order to show alteration of heat transfer enhancement and pressure drop in microchannels, not only modification in cross-section but also flow disruption techniques which interrupt thermal boundary layer and provides fluctuate fluid flow are studied by handled 5 models which have different corrugation with combining 3 various aspect ratio and sinusoidal functions. After this studies are carried out, the best efficient model which is selected in whole models will be determined.

1.2 Literature Review

Sui et al. (2011) performed experimental investigation on the flow friction and heat transfer in wavy microchannels using oblong transverse sections. The microchannel which is designed is composed of ten same wavy bodies which have 259 mm wavy amplitude, 2.5 mm wavelength, 404 mm depth and almost 205 mm width averagely. 60 – 62 wavy microchannels in collinear are involved by every test piece is produced of copper. Deionized water is selected as a working fluid also its Reynolds numbers are between 300 and 800. The experimental datum, primarily the average Nusselt number and friction factor, shows that wavy microchannels which has the identical cross section and floor space length has better than straight baseline microchannels in heat transfer performance. In the same breath, the heat transfer enhancement could be much bigger than wavy microchannels' the pressure drop penalty. Classical continuum approximation is fulfilled in the numerical investigation which has identical experimental constraints and the numerical datum conform rationally with experimental datum.

Mohammed et al. (2011) conducted numerically study in tortuous microchannel heat sinks, which have different amplitudes between 125 and 500 μm, in order to figure out heat transfer and flow properties. In the study, Reynolds number are chosen between 100 and 1000, also that flow is stationary, laminar and realistic is taken and

heat transfer governing equations are cleared up by utilizing the finite-volume method (FVM). Results which are taken from numerical study and include influence of utilizing tortuous structure on the thermal performance, the friction factor and wall shear stress are notified also are collated to the direct microchannel. To sum up, even though tortuous and direct microchannel have the identical transversal section, that heat transfer fulfilment is better in tortuous microchannel is determined. Owing to the fact that amplitude of tortuous microchannel is raised, wall shear stress and friction factor are raised moreover the heat transfer enhancement accomplishment of tortuous microchannels is few bigger than the pressure drop penalty.

Sui et al. (2012) carried out a study by using direct numerical simulation. In this study, flow is fully developed and microchannel geometry is selected as a wavy channel with rectangular cross section. Re number is increased with including both the steady laminar and transitional flow regions. While fluid flows past the bends, generation of symmetrical Dean vortices or secondary flows is monitored. Forms of secondary flows can develop on the flow direction, therefore this situation gives rise to chaotic advection which may extensively improve the convective fluid mixing and heat transfer. Moreover, increment in the Reynolds number induced the flow to change from steady state to periodic one with single frequency. In this step, the flow regime is formed by extremely complicated Dean vortices forms which develop momentarily and locationally on the flow direction, also symmetrical structure of the flow may even be vanished. This study shows us that the heat transfer performance is importantly more outstanding than straight channels which have the identical cross sections on the occasion of the efficacious mixing in wavy channels. Besides, the pressure drop penalty of wavy channels can be less than the heat transfer enhancement.

Ghani et al. (2017a) investigated a 3-D numerical simulation to analyze the features of fluid flow and heat transfer in microchannel heat sink, which has sinusoidal cavities and rectangular ribs (MC-SCRR), while Reynolds number is altered between 100 and 800. There are four main geometries and these are microchannel with rectangular MC-RC, microchannel with sinusoidal cavities MC-SC, microchannel with rectangular ribs MC-RR and MC-SCRR. The outcomes of analyses illustrate that MC-SCRR is more outstanding than MC-RR and MC-SC from the point of thermal performance. The latest layout of MC-SCRR has demonstrated the facility to

unify between two significant properties. One of them is wide flow field which importantly decreases the pressure drop and other one is high flow disruptions which are induced by existence of ribs in the central part of channel. The average performance of MC-SCRR is appraised in term of friction factor, Nusselt number and performance factor. The performance factor of MC-SRR is 1.85 at Re = 800.

Xia et al. (2013) examined numerical investigation of the features of water by way of the micro heat sink with fan-shaped reentrant cavities (FRCR) and internal ribs with various proportional rib height while Re number is altered between 150 and 600. Besides this investigation suggests empirical correlations of apparent friction factor and average Nusselt number for FRCR, also this is a function which is related to Reynolds number and proportional rib height. The consequences illustrate that in spite of that apparent friction factor is 6.5 times more than the rectangular microchannel, Nusselt number for FRCR is 1.3-3 times more. The contrasting of present statistics with the open data are illustrated that the unified influence of cavity and rib has more superior performance of heat transfer, also the influence of proportional rib height is more dominant than the single influence of the structure or the dimension of reentrant cavity while Reynolds number is higher than 300.

Kumar (2019) analyzed numerical investigation of fluid flow and heat transfer in a microchannel which type is a trapezoidal by utilizing finite volume method while Re number is altered between 96 and 720. In order to specify optimal heat flux dispersion through the microchannels, 3-D simulations were followed out at invariant heat flux and various pressure drop conditions. Besides, the attached influences of rectangular and semicircular sort grooves produced interior the microchannel were studied. Pressure drop is determined for extensive series of Reynolds number by experimentation and discovered contrasting satisfactory. It was found that the heat transfer in microchannel which has trapezoidal figured dramatically advanced by 12%, contrasted with the microchannel which has rectangular figured. In spite of the existence of grooves on the microchannel walls, the average Nusselt number were calculated as high with increment in Reynolds number together channel disturbances. Moreover, augmented influences of dimension and count of grooves were consistently studied in the microchannel which has trapezoidal shaped.

Abdul Hasis et al. (2018) accomplished numerical investigation of heat transfer and fluid flow which has fully developed and laminar regime in a microchannel which

has twisted sinusoidal wavy shaped. Incompressible, unsteady and 3-D model is utilized and in order to find the solution, finite volume method is applied with SIMPLE algorithm by keeping wall temperature and heat flux boundary conditions constant. Wide scale computations have been carried out to analyze the thermo-hydraulic performance of microchannels which have twisted wavy shaped by different amplitude of twist and wavelength ratios with Reynolds number which is altered between 300 and 700. Consequences demonstrates that the twisted microchannels can considerably augment heat transfer performance by inducing minimum pressure drop for low Reynolds number regime contrasted to microchannels which have sinusoidal shaped. Twisted microchannels which have greater aspect ratio and smaller waviness increased heat transfer augmentation of approximately 30% contrasted to sinusoidal wavy microchannels.

Ahmed et al. (2015) scrutinized a 3-D numerical investigation to analyze the influence of geometric variables on laminar flow and heat transfer features in grooved microchannel heat sink (GMCHS). Finite volume method is utilized in order to solve the governing and energy equations. In order to find optimum aluminum heat sink design, location of the cavities, pitch, tip length and the depth are considered. Nusselt number ratio, thermal/hydraulic performance and isotherm with streamline contours are taken into consideration to appraise the performance of GMCHS. Eventually, selected parameters which are presented in article provides Nusselt number augmentation of 51.59% and friction factor increment of 2.35%.

1.3 Hypothesis

The Nusselt Number is one of the important indicators in heat transfer enhancement. It depends on Re, Pr and geometric structure. If appropriate geometric modification is applied on microchannel, heat transfer enhancement can occur. Especially, alterations in direction of the flow are expected due to modifications which are on geometries. We hypothesize that each modification can not be a solution in order to augment heat transfer in comparison to straight channel, however optimum modification can be found with using different aspect ratio and wall structures.

2. FLUID FLOW AND HEAT TRANSFER IN MICROCHANNELS

2.1 Fundamentals of Microchannel Heat Sink

Internal flows have been researched area for many years. Not only man-made applications but also natural systems are given as examples for internal flows, such as aorta, alveolar ducts, capillaries, intestines, lungs, boilers, compact and heat exchangers (Kandlikar et al., 2006). Dimensions of these examples are shown in Figure 2.1.

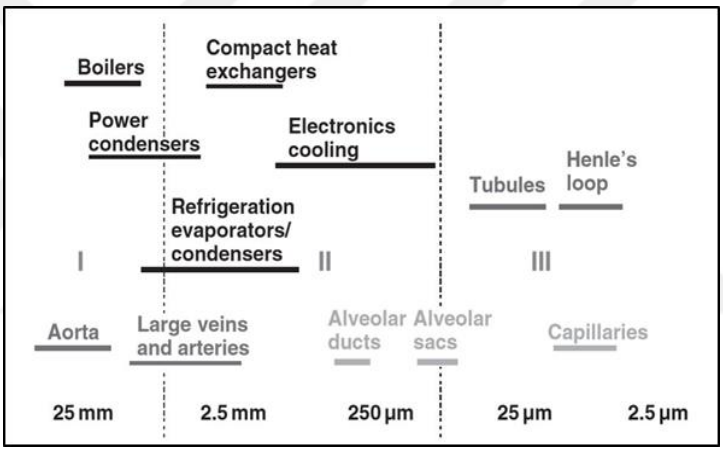

Figure 2.1 : Various applications (Kandlikar et al., 2006).

Microchannels which are some of them are research area which has been studied for 30 years. Especially, they are attracting topic associated with rapid growth in enhancement of ultra large scale integrated circuit (ULSIC) and Micro Electro Mechanical Systems (MEMS). According to (Kandlikar et al., 2002), channel classification is listed in Table 2.1.

Table 2.1 : Classification of channels (Kandlikar et al., 2002).

Channel Type	D (Smallest channel dimension)
Conventional channels	$D > 3$ mm
Minichannels	$3 \text{ mm} \geq D > 200$ µm
Microchannels	200 µm $\geq D > 10$ µm
Transitional Microchannels	10 µm $\geq D > 1$ µm
Transitional Nanochannels	1 µm $\geq D > 0.1$ µm
Nanochannels	0.1 µm $\geq D$

In microchannels, Knudsen number has importance in numerical investigations. No-slip boundary condition approach can not be chosen as a constraint all the time. After choosing the coolant in microchannel, in order to begin the computational section, Knudsen number must be calculated by formulation which is written in Equation (2.1).

$$Kn = \frac{\lambda}{H} \tag{2.1}$$

The meaning of λ is mean free path and H means characteristic length of channel. The mean space moved by a molecule between sequent clashes is the mean free path. It is shown in Figure 2.2.

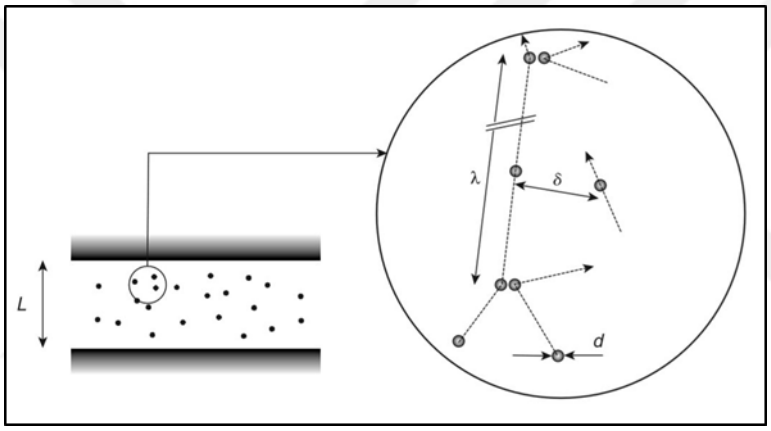

Figure 2.2 : Mean free path (Colin, 2013).

No-slip boundary constraint can be use in the continuum flow with Navier-Stokes (NS) equations. However, NS equations sustains feasible on the condition that a velocity slip and a temperature jump are considered at the walls. The continuum approach can not be used in transition flow regime, moreover intermolecular clashes must be considered so they are not ignored. Besides, in free molecular flow intermolecular collisions are ignored (Colin, 2013).

2.2 Heat Transfer Augmentation in Microchannels

Microchannels have higher heat transfer coefficient by reason of their low hydraulic diameter in spite of that it is in conjunction with superior pressure drop per unit dimension. The superior pressure gradients have orientated researchers to handle little flow rates. Nevertheless, along decreased the flow rate, the facility of removing temperature of the fluid stream grows into restricted. For augmentation of the

complete chilling performance, there are two alternatives. One of them is decreasing the flow length of the channels and the second one is enhancing the liquid debit (Kandlikar et al., 2002). Alteration of heat transfer coefficient and pressure gradient with passage dimension for a chequer passage under laminar flow, invariable heat flux boundary constraint, supposing no rarefaction and compressibility influences are displayed in Figure 2.3 and Figure 2.4, respectively.

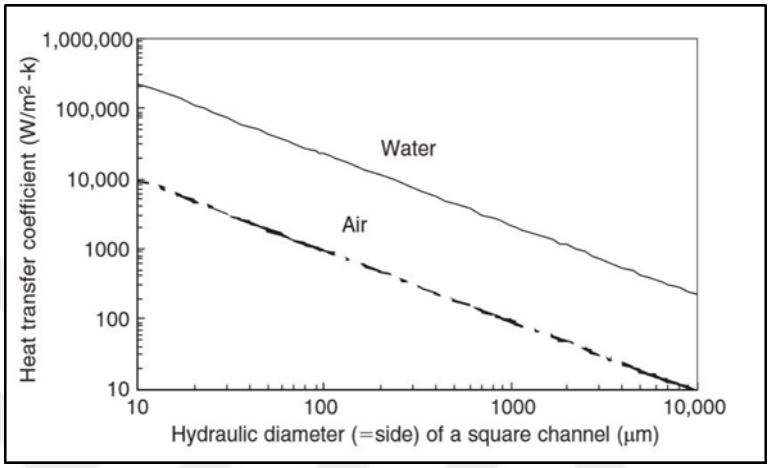

Figure 2.3 : Alteration of heat transfer coefficient (Kandlikar et al. 2006).

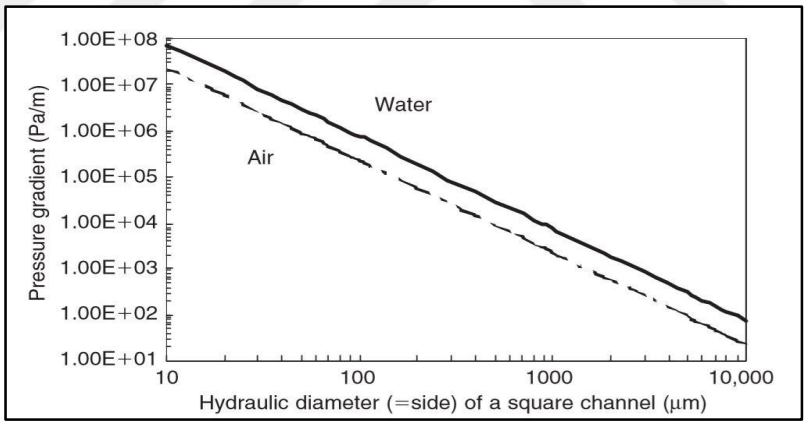

Figure 2.4 : Alteration of pressure gradient (Kandlikar et al. 2006).

2.2.1 Curled channel

The modification in geometry of microchannels can be observed as curled structure. In this adjustment, there is no local alterations which can be called as cavities, ribs and fin. Instead of them, side walls of the microchannel is curved in many different shapes. Cross-section is not changed but curled structure is obtained in order to provides generation of Dean vortices (Secondary Flow). There are two main curled structure in microchannels. One of them is zigzag channels and other one is wavy microchannel.

Zheng et al., (2014) studied the flow and heat transfer enhancement in repeated zigzag channels which are shown in Figure 2.5 and Figure 2.6. In transient regime, velocity of the flow usually oscillates in the tortuous passages with a semi-circular haphazardly. Re number is varied between 400 and 800. Oscillated structure caused different vortex forms on the both cross-section areas. Due to vortex structures, remarkable heat transfer enhancement is succeeded.

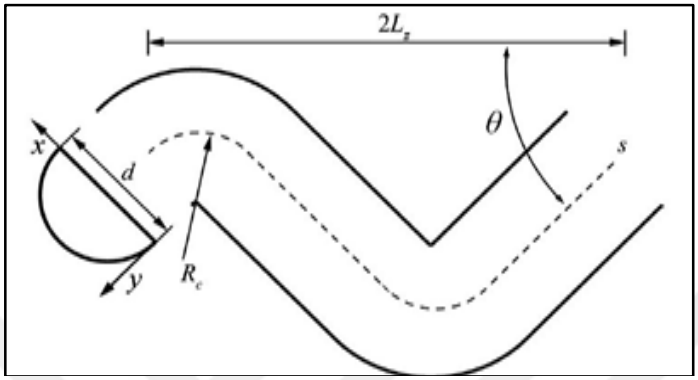

Figure 2.5 : The zigzag microchannel (Zheng et al., 2014).

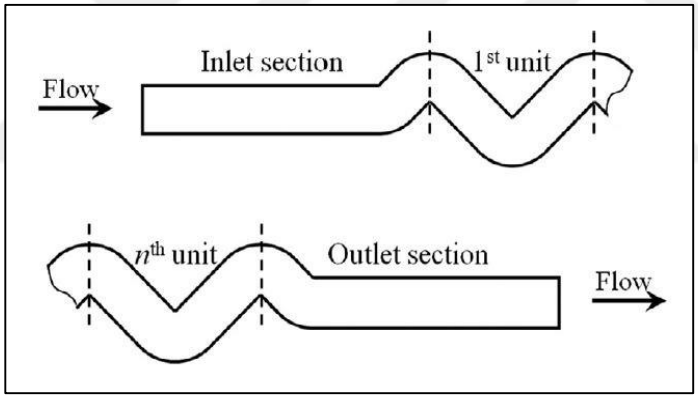

Figure 2.6 : Sections in the zigzag microchannel (Zheng et al., 2014).

2.2.2 Flow disruption

As a heat transfer enhancement procedure, flow disruption is brought out based on the inducing of flow imbalances which is in charge of augmented flow mixing and augmentation of heat transfer. As an accustomed instance, turbulent flow can be declared. Due to poor velocities and low hydraulic diameter, flow is unqualified to figure out at critical Reynolds number in numerous practices. Therefore, devoted endeavors are performed to increasing the flow imbalances and enhanced mixing by employing dimensional alteration to the boundaries of channels. That repeated perturbation promoters which can be grooves, fins and ribs are arranged throughout the flow way is an effective procedure to gain features which are mentioned above.

These perturbation promoters are set up to get efficacious for inducing the self-sustained vibrations that stimulate flow imbalances (Ghani, et al., 2017). Many researchers which utilize perturbation promoters in their studies focus on improving the flow imbalance, mixing and interruption of thermal-hydraulic boundary layer.

2.2.3 Surface roughness and reentrant obstacles

In order to enhance the heat transfer in microchannels, some assistant modifications are utilized such as cavities, ribs, dimple and fins as seen in Figure 2.7. In this section these structures are scrutinized with studies which are found in literature.

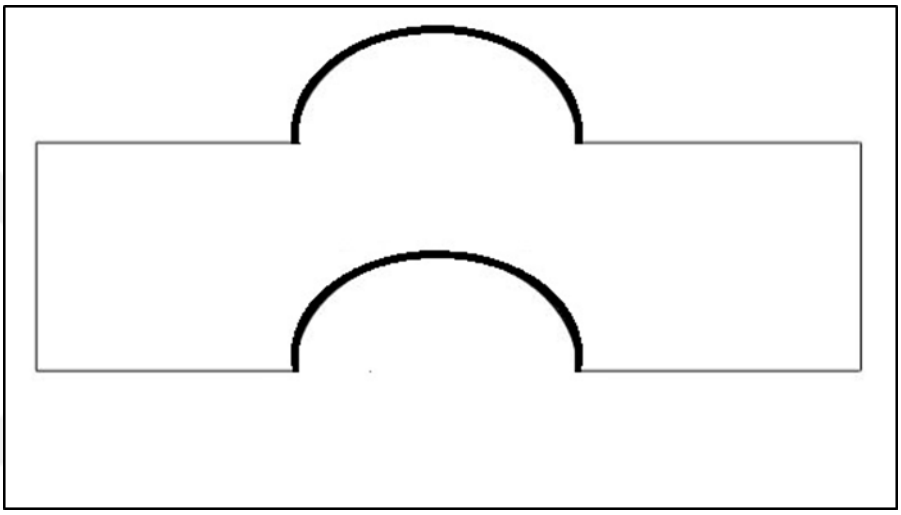

Figure 2.7 : Cavity and rib structures.

Fins which can interrupt thermal-hydraulic boundary layer are very useful obstructions. Dimensional modification is preferred for fins such as rectangular prism shaped and cylinder shaped.

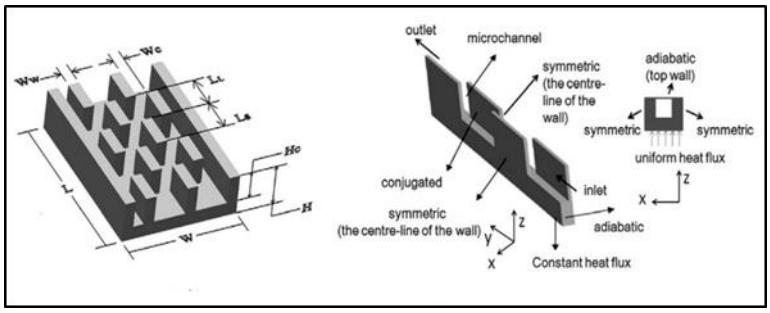

Figure 2.8 : Fins in the microchannel (Hong & Cheng, 2009).

Hong and Cheng, (2009) performed numerical investigation of conjugate heat transfer by using offset strip-fin which is shown in Figure 2.8 for microelectronic cooling. As a result, by virtue of repeated alteration of the flow direction, the

convective heat transfer is augmented by mixing cool and hot refrigerant, also the repeated interruption of boundary layer is other consideration to augment heat transfer.

3. MATHEMATICAL MODEL OF MICROCHANNEL HEAT SINK

3.1 Governing Equations

In order to solve conjugate heat transfer and fluid flow in microchannels which have different geometric shapes in this thesis study, some assumptions are accepted. The flow is incompressible, steady and laminar. The effects of gravity and radiation heat transfer are negligible. That flow has no-slip boundary conditions is considered. Excluding water viscosity which depends on temperature, other properties for solid and fluid are considered as constant. The influence of viscous dissipation of fluid is negligible.

For fluid region, continuity, momentum and energy equations are shown in Equations (3.1), (3.2) and (3.3), respectively.

$$\nabla \vec{V} = 0 \tag{3.1}$$

$$\rho_f \left(\vec{V}.\nabla \vec{V}\right) = -\nabla p + \nabla.\left(\mu_f \nabla \vec{V}\right) \tag{3.2}$$

$$\rho_f c_{p,f} \left(\vec{V}.\nabla T_f\right) = k_f \nabla^2 T_f \tag{3.3}$$

For solid region, energy equation is shown Equation (3.4).

$$k_s \nabla^2 T_s = 0 \tag{3.4}$$

In this problem, viscosity is considered as a property which changes depending on temperature which is denoted by T by using formula of Kestin et al. (1978). This is formula is represented in Equation (3.5).

$$\log\left\{\frac{\mu(T)}{\mu(20°\mathrm{C})}\right\} = \frac{20-T}{T+90}\{1.2378 - 1.303\times 10^{-3}(20-T) + 3.06 \times 10^{-6}(20-T)^2 + 2.55\times 10^{-8}(20-T)^3\} \tag{3.5}$$

Reynolds Number impresses with Prandtl Number to Nusselt Number directly. In order to determine inlet velocity for mathematical model, the following Equation (3.6) is used. Besides, Pr is calculated by Equation (3.7)

$$Re = \frac{\rho_f \times u_{in} \times D_h}{\mu_{in}} \tag{3.6}$$

$$Pr = \frac{\mu \times c_p}{k_f} \tag{3.7}$$

In order to determine friction effects, the fanning friction factor is calculated by using the following Equation (3.8).

$$f = \frac{\tau_w}{\frac{1}{2} \times \rho_f \times u_m^2} \tag{3.8}$$

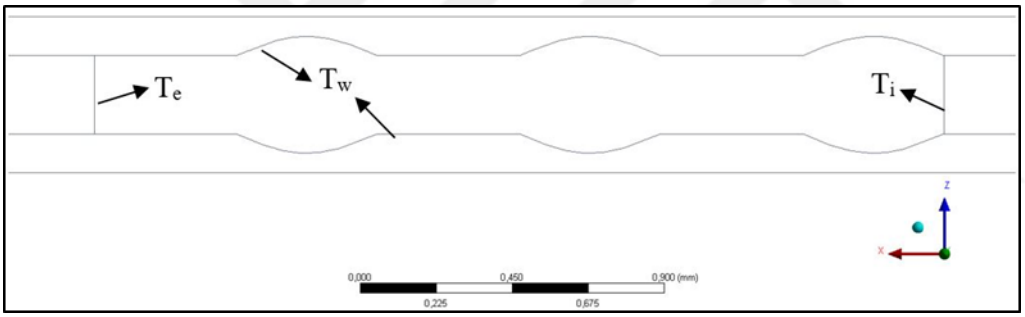

Figure 3.1 : Mathematical model of M1_F2_AR1.

Area-weighted average inlet and exit temperature are calculated then temperature difference is found by using the following Equation (3.9).

$$\Delta T_1 = T_e - T_i \tag{3.9}$$

Energy balance is written in order to calculate heat which transferred from walls to the coolant in Watt unit by using Equation (3.10).

$$\dot{q} = \dot{m} \times c_p \times \Delta T_1 \tag{3.10}$$

Mass flow rate is variable in this problem; it can be calculated by Equation (3.11).

$$\dot{m} = \rho \times u_{in} \times A_f \tag{3.11}$$

After finding heat transfer amount, in order to find heat transfer coefficient, the following Equation (3.12) is utilized.

$$h_{avg} = \frac{q}{A_{fs} \times \Delta T_2} \tag{3.12}$$

The temperature differences between wall and coolant must be calculated to reach heat transfer coefficient. It is calculated in the Equation (3.13).

$$\Delta T_2 = T_{w,ave} - T_{f,ave} \tag{3.13}$$

By using heat transfer coefficient and hydraulic diameter with thermal conductivity, Nusselt number can be found in the Equation (3.14).

$$Nu = \frac{h_{avg} \times D_h}{k_f} \tag{3.14}$$

In order that calculated Nusselt number has a meaning, x^+ values must be calculated for each sub-case by using Equation (3.15)

$$x^+ = \frac{x/D_h}{Re \times Pr} \tag{3.15}$$

In order to compare models' influences on the heat transfer enhancement, correction coefficients must be used for each comparison. Fanning friction coefficient (f) is shown symbolized with f. Nu number depends on Re, Pr and geometric structure. These situations can be shown in Equation (3.16) and (3.17).

$$Nu = F(Re, Pr, Geo) \tag{3.16}$$

$$f = F(Re, Geo) \tag{3.17}$$

In order to observe influences of the modification, these correction coefficients are used for finding value which is divided by values of models.

$$Nu_o^* = Nu_o \times \left[\frac{Re_m \times Pr_m}{Re_o \times Pr_o}\right]^{\frac{1}{3}} \tag{3.18}$$

$$f_o^* = f_o \times \frac{\frac{1}{Re_m}}{\frac{1}{Re_o}} \tag{3.19}$$

Finally, in order to the modificated models can be contrasted to straight microchannels, PEC number is used. For each model, Nu_o^* and f_o^* are calculated then PEC number is calculated in Equation (3.20) (Bayrak et al., 2019).

$$PEC = \frac{Nu/Nu_o^*}{(f/f_o^*)^{\frac{1}{3}}} \tag{3.20}$$

3.2 Models

In this study, a straight microchannel and assorted microchannels which has corrugation configuration were assessed by comparative analogy. There are totally 3 various models except a straight microchannel. Each model has 3 different aspect ratios which are 1/3, 1 and 3 in return. Equation (3.21) gives aspect ratio, a and b are denoted by height and wide respectively.

$$AR = \frac{b}{a} \tag{3.21}$$

Three various sinusoidal functions are used for each model. These functions are shown in Equations (3.22) -(3.24).

$$F1 = 0.05775 \times \sin(5x) \tag{3.22}$$

$$F2 = 0.05775 \times sin(7.5x) \tag{3.23}$$

$$F3 = 0.05775 \times sin(15x) \tag{3.24}$$

Entrance length is calculated for each straight microchannels which have different aspect ratios by using Equations (3.25) and (3.26).

$$D_h = \frac{4 \times Volume}{Surface\ Area} \tag{3.25}$$

$$\frac{L_h}{D_h} = 0.05 \times Re \tag{3.26}$$

Table 3.1 : Hydraulic entrance length (L_h) values

Aspect Ratio (AR)	Re	a (μm)	b (μm)	D_h (μm)	L_h (mm)
1/3	200	693	231	346.5	3.465
1	200	231	231	231	2.310
3	200	77	231	115.5	1.155

Keeping wide length of all models, other variable parameters are displayed in Table 3.1. The sinusoidal functions for each microchannels corrugated are begun in 7 mm for each microchannel. Also, they continue throughout only 4π/5 mm in microchannels.

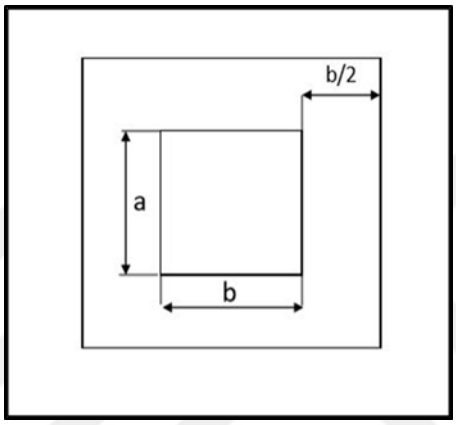

Figure 3.2 : Cross-section of each sub-case.

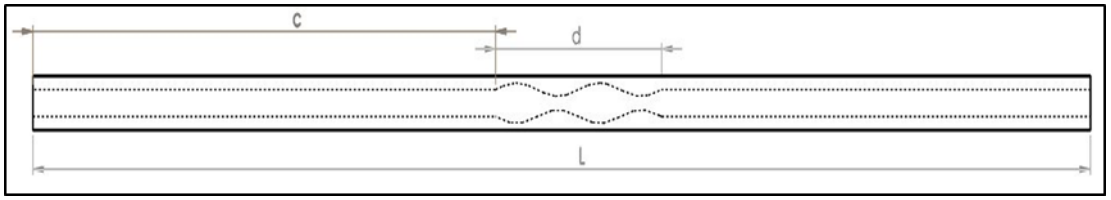

Figure 3.3 : Top view of M2_F1_AR1.

Cross-section and other parameters are displayed in Figure 3.3 and Figure 3.4. Table 3.2 gives us that each sub-case has constant b, c, d and L values but a is various for each sub-case which have different aspect ratios.

Table 3.2 : Dimensions of parameters in different channels which have various aspect ratios.

Aspect Ratio (AR)	a (μm)	b (μm)	c (mm)	d (mm)	L (mm)
1/3	693	231	7	4π/5	16
1	231	231	7	4π/5	16
3	77	231	7	4π/5	16

3.2.1 Model 1

In this model, sinusoidal functions behave as half-wave rectifier connected. Besides, sinusoidal waves are symmetrically located in the microchannel. There are 9 different microchannels in Model 1. Because of that top views are small in the microchannels which have same function and different aspect ratios. These are shown in Figure 3.4, Figure 3.5 and Figure 3.6.

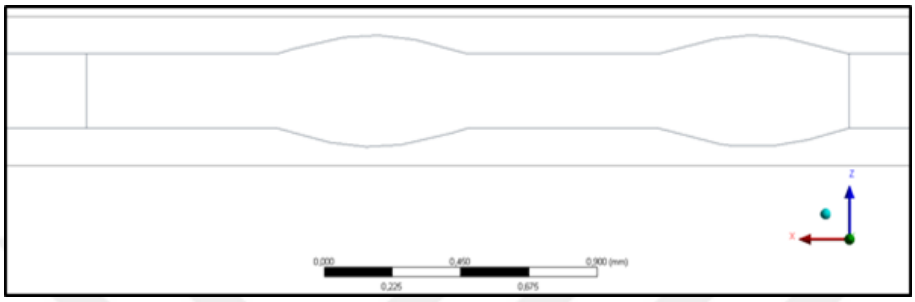

Figure 3.4 : Top view of M1_F1_AR1.

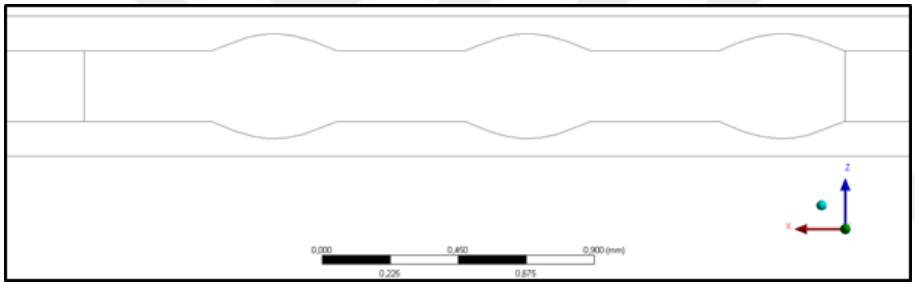

Figure 3.5 : Top view of M1_F3_AR1.

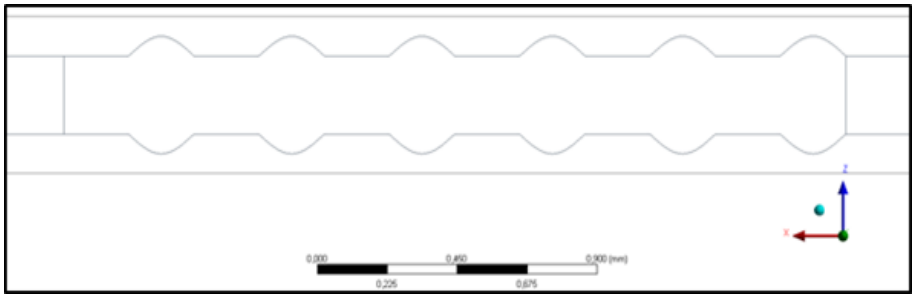

Figure 3.6 : Top view of M1_F3_AR1.

3.2.2 Model 2

In this model, sinusoidal functions act as full wave. Moreover, sinusoidal waves are placed in bilateral structure. This model has 9 different kinds of geometric shape like Model 1. Three different aspect ratios are used by combining with 3 different functions which are mentioned on numerical models. Some of these are displayed in Fig. 3.7, Fig. 3.8 and Fig. 3.9.

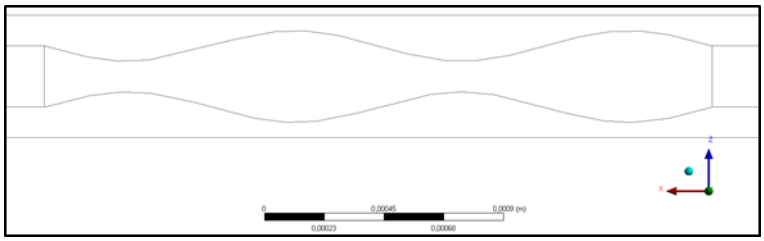

Figure 3.7 : Top view of M2_F1_AR1.

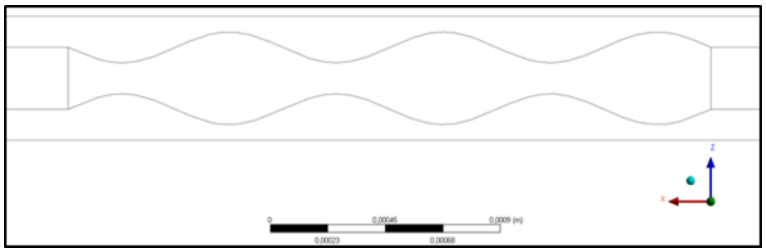

Figure 3.8 : Top view of M2_F2_AR1.

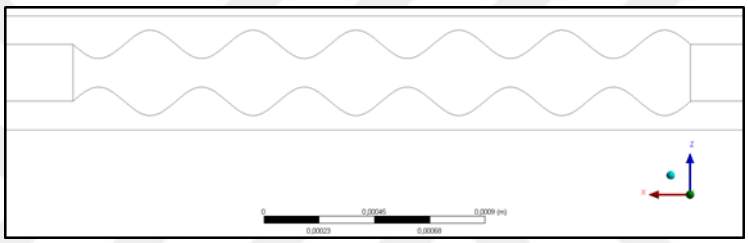

Figure 3.9 : Top view of M2_F3_AR1.

3.2.3 Model 3

In this model, sinusoidal functions build wavy shape. Furthermore, sinusoidal waves are located as one under the other. Some like other models, Model 3 has 9 different sub-models. Some of these are shown in Figure 3.10, Figure 3.11 and Figure 3.12.

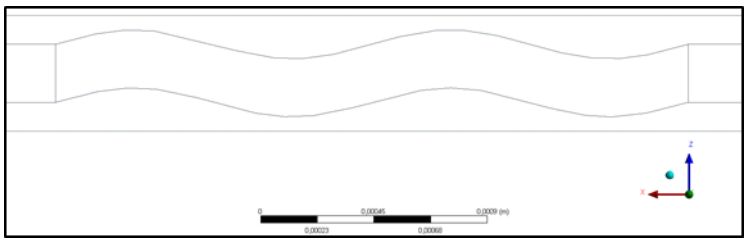

Figure 3.10 : Top view of M3_F1_AR1.

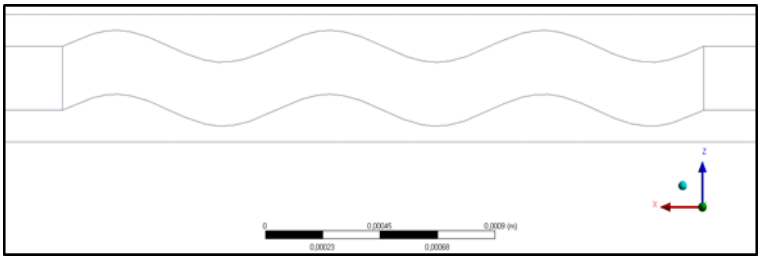

Figure 3.11 : Top view of M3_F2_AR1.

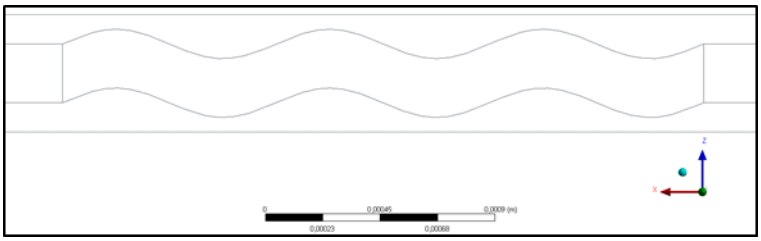

Figure 3.12 : Top view of M3_F3_AR1.

3.2.4 Model 4

In this model, sinusoidal functions behave as half-wave rectifier connected like Model 1. Nevertheless, instead of symmetrical structure, non-symmetrical arrangement is used. Model 4 has 9 sub-cases like others. Some of them are displayed in Figure 3.13, Figure 3.14 and Figure 3.15.

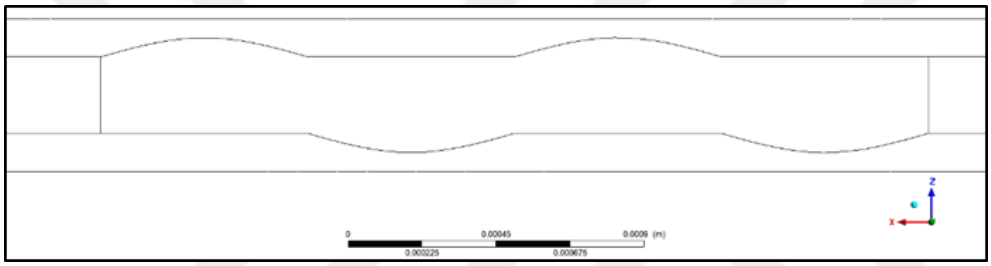

Figure 3.13 : Top view of M4_F1_AR1.

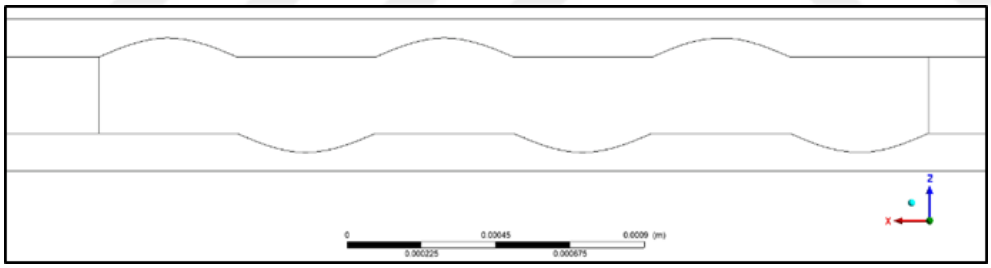

Figure 3.14 : Top view of M4_F2_AR1.

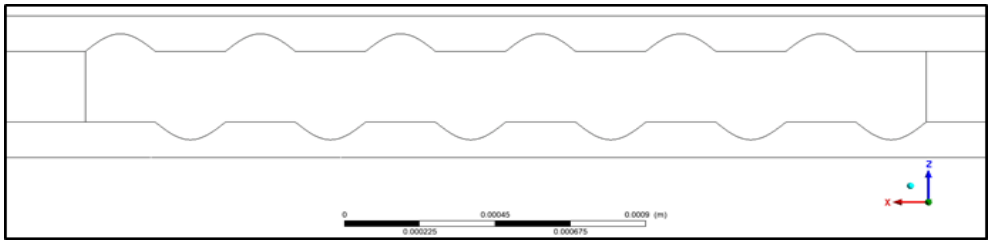

Figure 3.15 : Top view of M3_F3_AR1.

3.2.5 Model 5

Model 5 is considered as a reverse of Model 4 with 9 various sub-cases. Some of them are shown in Figure 3.16, Figure 3.17 and Figure 3.18.

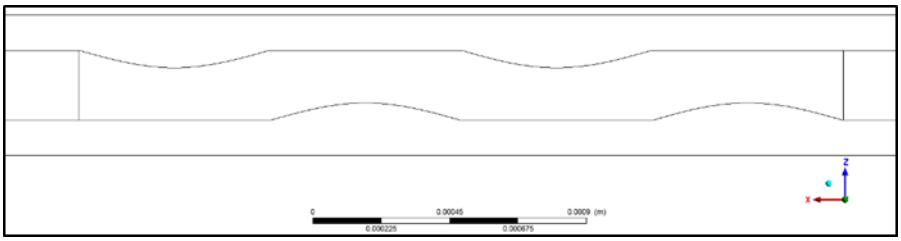

Figure 3.16 : Top view of M5_F1_AR1.

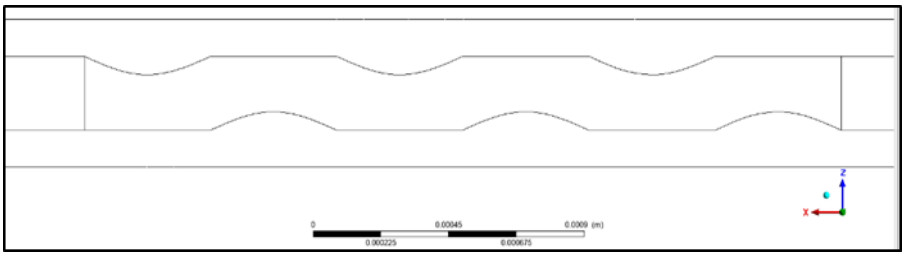

Figure 3.17 : Top view of M5_F2_AR1.

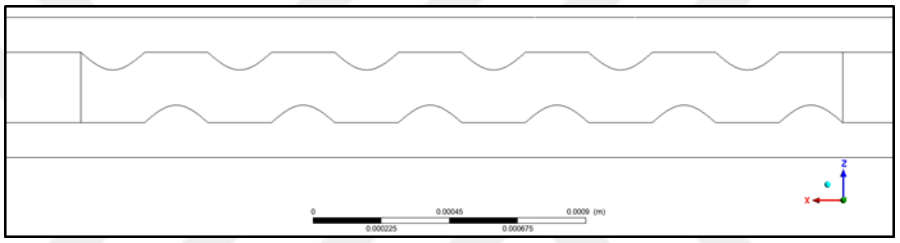

Figure 3.18 : Top view of M5_F3_AR1.

4. VALIDATION

The study of Wang et al. (2016) was selected for validation of this study by investigating pressure drop and temperature distribution. Figure 4.1 demonstrates the geometry of the model. Model is conjugate and it has fluid and solid part. Dimensions of fluid part are 0.231 x 0.713 x 44.8 mm^3 and dimensions of solid part are 7.62 x 0.462 x 44.8 mm^3. In this simulation, the heat flux which is applied from only bottom wall is applied as constant, q = 100 W/cm^2 and other walls are assumed as adiabatic, inlet temperature of cooling water T_{in} = 288.15 K and inlet velocity u_{in} is variable depending upon Reynold number which varies between 100 and 1600. In this study, The Finite volume method is carried out and the conjugate heat transfer problem is tried to solve by using SIMPLEC algorithm. Second order upwind scheme is chosen to discretize energy and momentum equations. Residuals for continuity, velocities and energy are selected 1 x 10^{-4}, 1 x 10^{-4}, 1 x 10^{-7} in return to find out solutions as converged. Thermophysical properties of heat sink substrate and fluid are shown in Table 4.1.

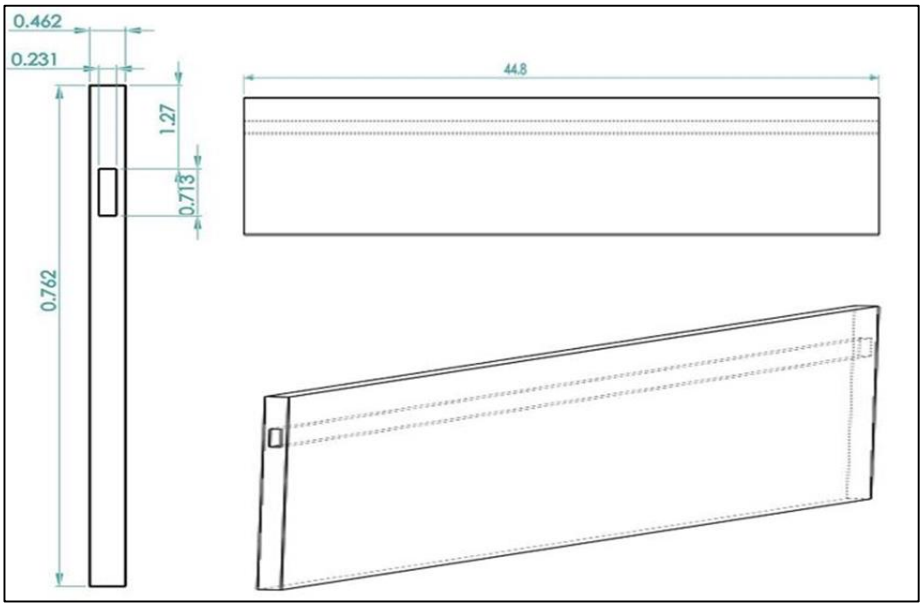

Figure 4.1 : Different views of the validation model.

Table 4.1 : Thermophysical properties of heat sink substrate and fluid.

Materials	Density (kg/m3)	Thermal conductivity (W/mK)	Specific heat (J/kgK)
Water	1000	0.6	4178
Copper	8933	401	385

In this study, viscosity is not accepted constant and that it changes with altering of temperature is accepted. Therefore, water viscosity is calculated from Equation (3.5) shown by Kestin et al. (1978). As it is seen from Table 4.2, temperature changing can not be neglected.

Table 4.2 : Dynamic viscosity values at different temperatures.

T (°C)	μ_{in} (kg/m.s)
15	1.14×10-3
20	1.00×10-3
25	8.83×10-4
30	7.87×10-4

Also Table 4.3 is prepared to show changing of inlet velocity related to Reynolds number by using Equation (3.6). In order to show effects of temperature on viscosity, an udf is written appropriately by using codes which are compatible with Ansys Fluent 19.2 solver. Mesh independence is applied by using 4 different mesh types.

Table 4.3 : Mean velocities values at different Reynolds Numbers.

Re	u_{in} (m/s)
100	3.266×10-1
200	6.533×10-1
300	9.799×10-1
400	13.07×10-1
500	16.33×10-1
600	19.60×10-1
700	2287×10-1
800	26.13×10-1
900	29.40×10-1
1000	32.66×10-1
1100	35.93×10-1
1200	39.20×10-1
1300	42.46×10-1
1400	45.73×10-1
1500	49.00×10-1
1600	52.26×10-1

These meshes are shown in Table 4.4 with their number of divisions. Bias value is 3 and mesh method is multizone. Location of mesh parameters and mesh structure are shown in Figures 4.2. and 4.3, respectively.

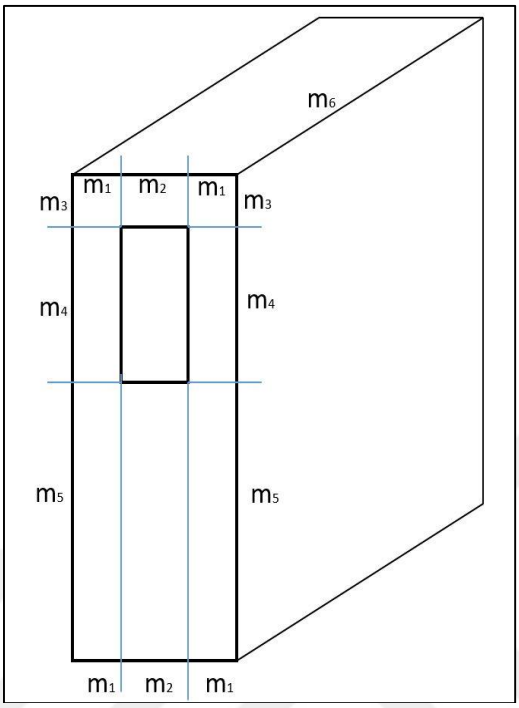

Figure 4.2 : Locations of mesh parameters.

Table 4.4 : Number of division for mesh parameters

Mesh Type	m_1	m_2	m_3*	m_4*	m_5	m_6
1	5	48	24	72	240	1200
2	4	40	20	60	200	1000
3	4	30	15	45	150	750
4	4	20	10	30	100	500

*Bias

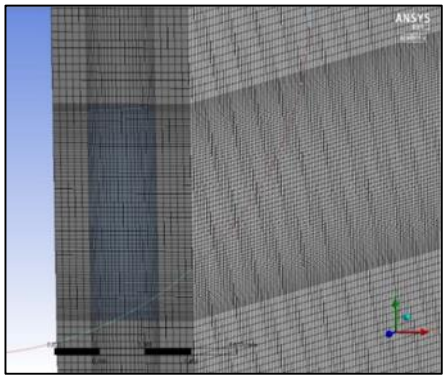

Figure 4.3 : Mesh structure.

In order to find optimum mesh type, relative error is calculated for each one except the finest mesh by using Equation (4.1).

$$e = \left| \frac{P_e - P_o}{P_e} \right| \tag{4.1}$$

In Equation (4.1), P_e is used for pressure drop of model which has coarser mesh type, moreover P_o means pressure drop of model which has more fine mesh. Mesh_3 was selected for investigations.

Table 4.5 : Mesh independence study results.

Mesh Type	Element Number	Pressure Drop (bar)	e (relative error)
Mesh_1	14.688×106	0.04460	-
Mesh_2	8.4×106	0.04442	0.353
Mesh_3	3.88125×106	0.04415	0.641
Mesh_4	1.35×106	0.04335	1.817

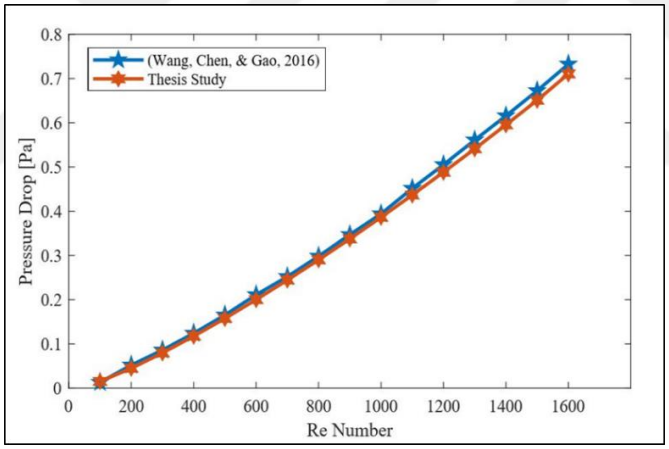

Figure 4.4 : A comparison between thesis study and (Wang et al., 2016).

According to Figure 4.4, the numerical analysis of thesis study and Wang et al. (2016) pressure drop values are very close to each other.

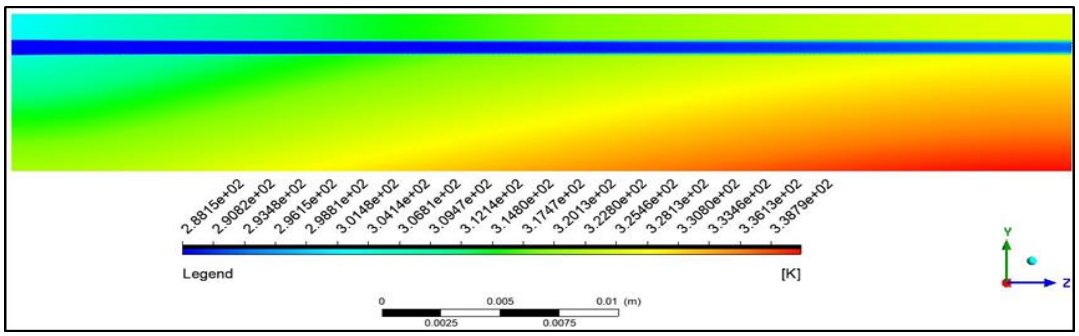

Figure 4.5 : Temperature distribution of thesis study.

Also, the temperature distributions of thesis study and validated model are similar as seen in Figure 4.5 and Figure 4.6.

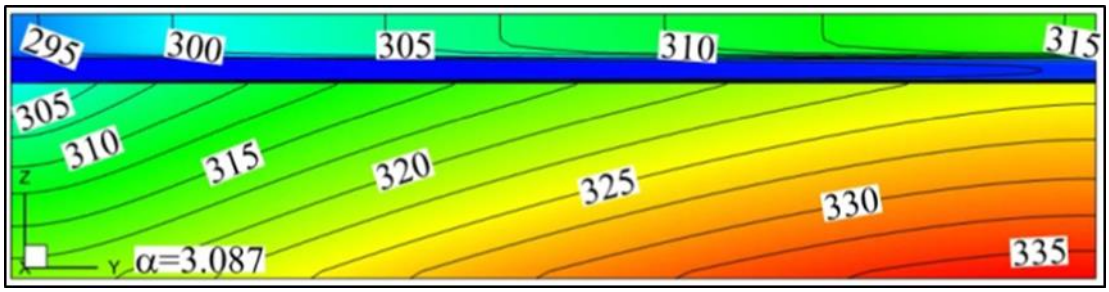

Figure 4.6 : Temperature distribution of (Wang et al., 2016).

5. ANALYSES OF DIMENSIONAL INFLUENCES

In this thesis study, the conjugate heat transfer models are designed and solved by using Solidworks 2018 and Ansys Fluent 19.2. Also, C programming language is utilized for user define function (UDF) which enables program to reflect influences of temperature on viscosity changing. Moreover, udf which is written for dynamic viscosity locates in Appendix B. For each models, the heat flux is implemented under the bottom wall as constant, $q"$= 20 W/cm^2 and other solid surfaces are considered as adiabatic. Thermal conductivity of the coolant is selected as temperature dependent on the contrary of validation model. Besides, viscosity of the coolant depends on alteration of temperature according to the formula of Kestin et al. (1978). In whole channel's inlet temperature of fluid T_{in} = 298.15 K. Solid part is Aluminum and fluid part is selected as water.

Re number is picked as 200 and inlet velocities u_{in} which are calculated using Equation (3.6) are determined according to aspect ratio as seen in Table 5.1.

Table 5.1 : Mean velocities corresponding to various aspect ratios.

Aspect Ratio (AR)	u_{in} (m/sn)
1/3	0.5106
1	0.7659
3	1.532

In order to obtain precious results from series of analysis, true mesh structure must be determined before starting numerical investigations. Therefore, mesh independence study was conducted by choosing M2_F3_AR1. Because, this case includes both converging and diverging structure which has sophisticated mesh structure in comparison to other cases.

5.1 Mesh Independence Study

In order to gain optimum mesh structure, 5 different mesh structures are applied on M2_F3_AR1 which is shown with front and top views in Figures 5.1 and 5.2,

respectively. These structures have different sensibility and element number. Used dimensions are shown in Table 5.2.

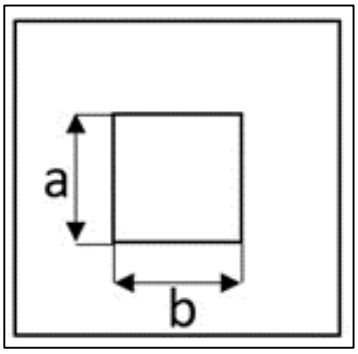

Figure 5.1 : Cross-section.

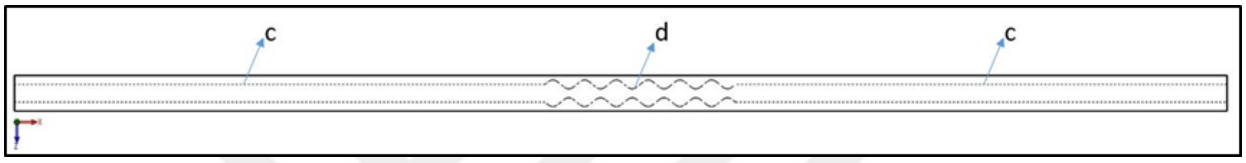

Figure 5.2 : Top view of M2_F3_AR1.

In order to find optimum mesh type, relative error is calculated by using Equation (5.1) for each mesh type except the finest mesh type which is Mesh_1.

Table 5.2 : Mesh types for mesh indepence study.

Mesh Type	a ($x10^{-3}$)	b ($x10^{-3}$)	c ($x10^{-3}$)	d ($x10^{-3}$)	Mesh Size (Solid)	Element Number ($x10^{6}$)
Mesh_1	5.775	5.775	5.775	1.5	$7x10^{-3}$	7.092096
Mesh_2	6.6	6.6	6.6	1.5	$8x10^{-3}$	5.183630
Mesh_3	7.7	7.7	7.7	1.5	$9x10^{-3}$	3.805851
Mesh_4	9.24	9.24	9.24	1.5	$11x10^{-3}$	2.489592
Mesh_5	11.55	11.55	11.55	1.5	$13x10^{-3}$	1.576364

Table 5.3 : Pressure Drop and e value corresponding to mesh types.

Mesh Type	Pressure Drop	e
Mesh_1	3432.284	-
Mesh_2	3437.168	0.14
Mesh_3	3449.711	0.36
Mesh_4	3483.992	0.99
Mesh_5	3590.580	3.05

According to the Table 5.3, Mesh_2 was selected because of the lowest error range (e). This mesh structure can be observed in Figure 5.3 and Figure 5.4. The other mesh types are displayed in Appendix A. However, mesh structure of all cases for

fluid part are same but solid part mesh structures of all cases are not same because of various functions.

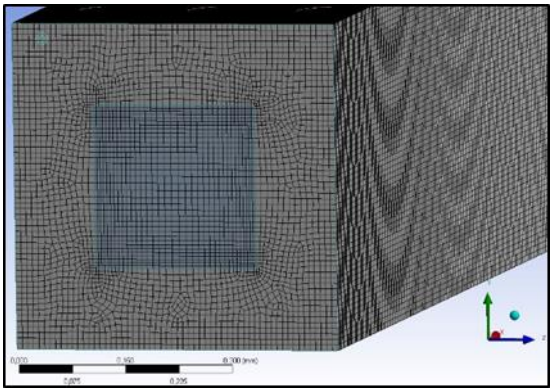

Figure 5.3 : Mesh structure for the front view of the model.

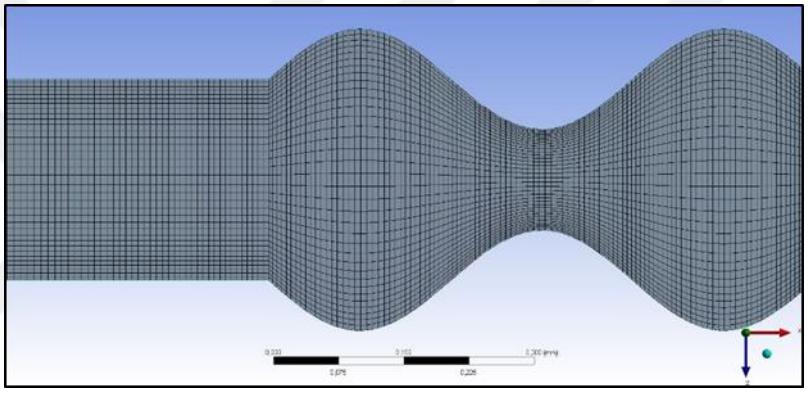

Figure 5.4 : Mesh structure for the top view of the model.

5.2 Models

In this section, the results which are taken from each model are given. First of all, the straight microchannel are analyzed with 3 different aspect ratios in order to Nusselt Number and skin wall friction, moreover outcomes are displayed in Table 5.4.

Table 5.4 : Nu_o and f_o values with x^+ corresponding to various aspect ratio for straight microchannels.

Case Type	Nu_0	f_0	x^+(mm)
MR_AR1/3	5.59	0.076	0.016
MR_AR1	4.33	0.058	0.025
MR_AR3	4.94	0.067	0.050

According to x^+ values which are calculated by Equation (3.15) at seventh millimeter from the beginning, none of them has developed thermal boundary layer. Therefore, thermal-entry length problem is our main phenomena.

5.2.1 Model 1

In this model, only influences of cavity structure are examined. The reentrant cavity structures provide flow separations in grooves and boundary layer interruption is procured in each beginning of cavities. One of cases which are investigated is displayed in Figure 5.5.

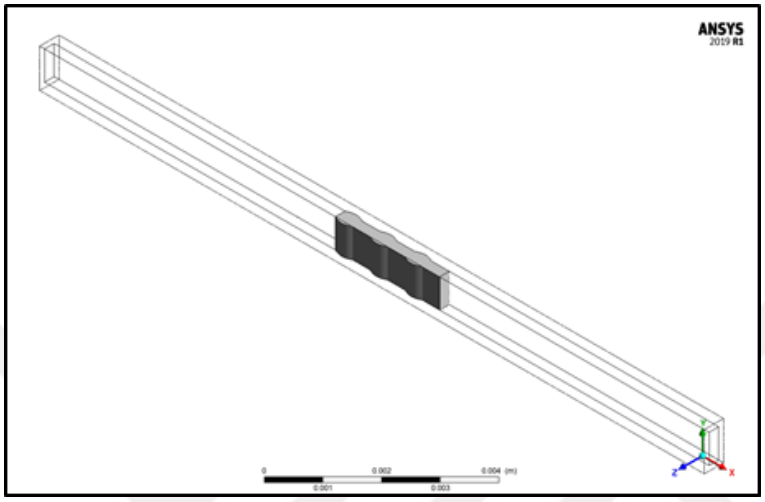

Figure 5.5 : Calculated Volume of M1_F2_AR1/3.

9 different cases which belong to Model 1 are investigated and Nu and f values are shown in Table 5.5, Table 5.6 and Table 5.7. For each sub-case, center horizontal plane is taken and flow characteristics are observed, the view of the central horizontal plane is given in Figure 5.6.

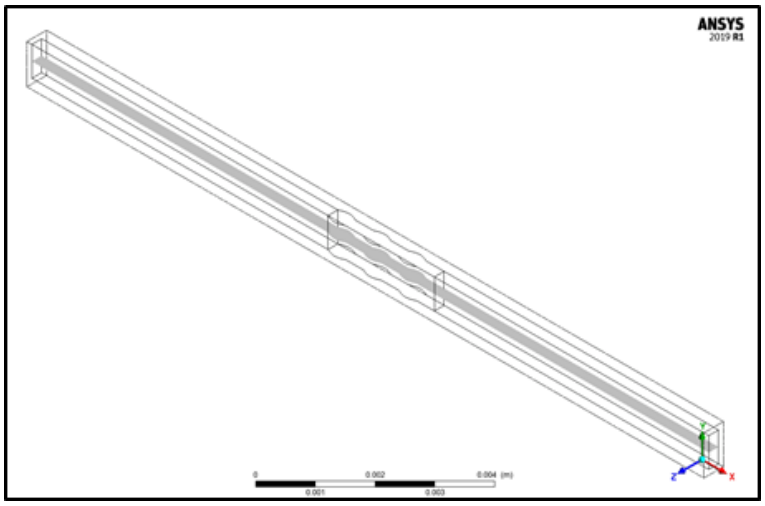

Figure 5.6 : The central horizontal plane in M1_F2_AR1/3.

In our series of numerical analysis, jet-like flows are observed in the reentrant cavities. Pressure values increase at specific zones due to jet-like flows.

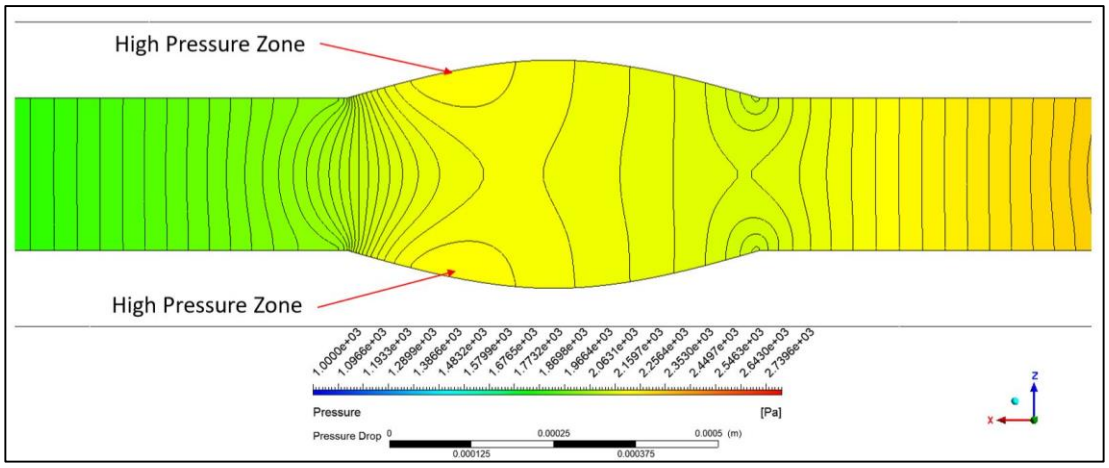

Figure 5.7 : Pressure Drop in the second cavity of M1_F1_AR1.

The pressure drops dramatically throughout the microchannel because of viscous effects. In the regions of instant enlargement, pressure dramatically increases as seen in Figure 5.7. Especially, at the front side of the reentrant cavities the pressure is superior than the circumjacent areas to improve the opposite pressure gradient (Xia et al., 2011). Vortices are produced under favour of fluid friction and separation. Thus, in order to produce particular vortices, exclusive surfaces are essential. There are two properties of vortices. These properties augment transport procedures which swirl and break stabilization of the flow region, in this way unstable or turbulent flow occurs (Fiebig, 1995).

Recirculation zones which are shown in Figure 5.10 are watched in cases which have F3 unlike cases which have F1 and F2 as seen in Figures 5.8 and 5.9. In M1_F3_AR1 the fluid flow is so slow and this situation reduces the heat transfer enhancement, therefore it is an unwelcome phenomenon. For this model, increment in frequency induces this problem.

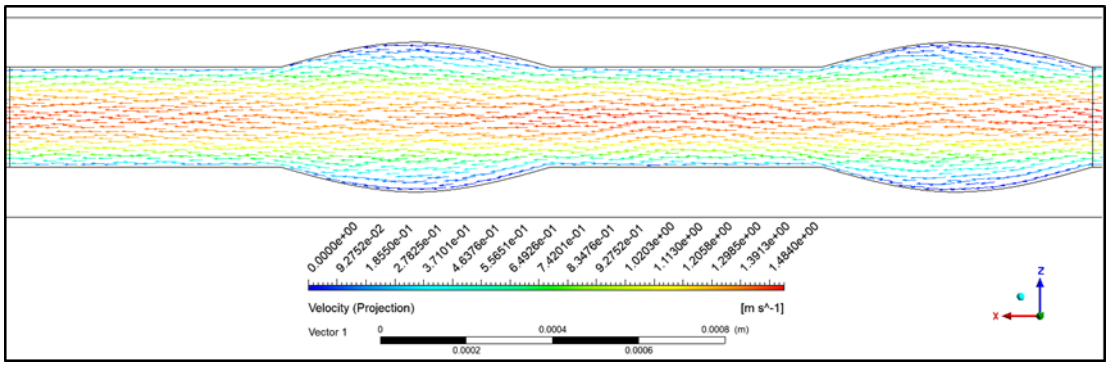

Figure 5.8 : Velocity vectors in M1_F1_AR1.

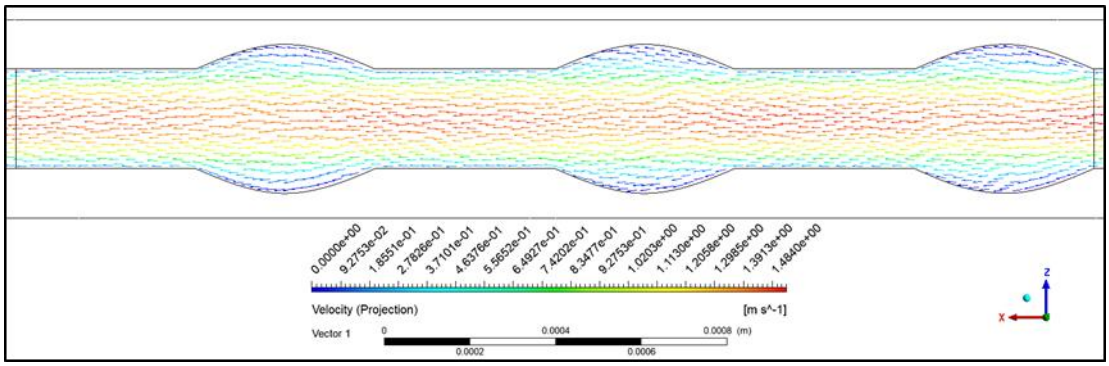

Figure 5.9 : Velocity vectors in M1_F2_AR1.

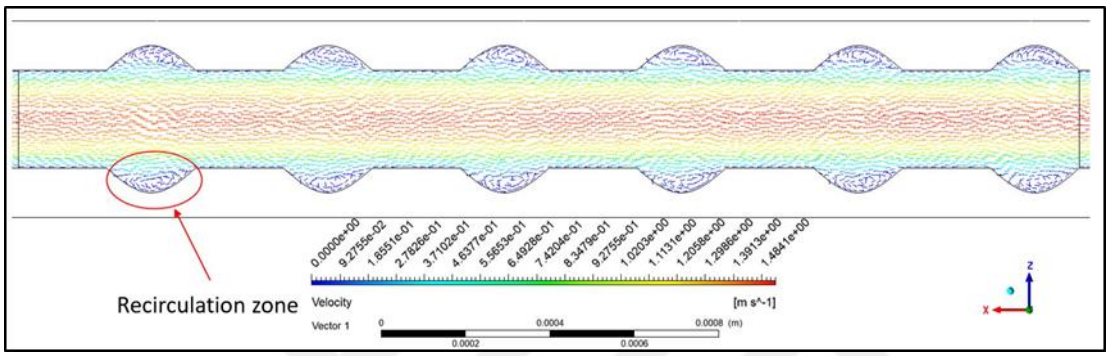

Figure 5.10 : Velocity vectors in M1_F3_AR1.

Regardless of the the fact that there is recirculation structure, the reentrant cavities generate swirl flow. In order to observe this swirl, a vertical plane is taken each model just like Figure 5.11.

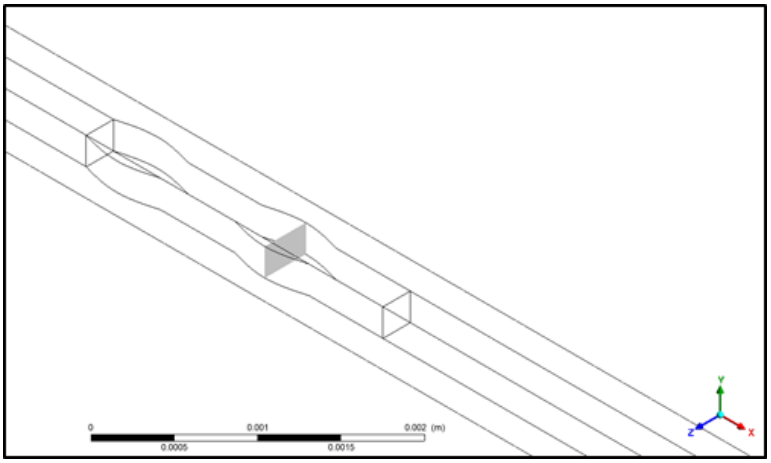

Figure 5.11 : The vertical plane in M1_F1_AR1.

Swirl flow provides mixing which occurs between cool and heated coolant particles. This causes better convection heat transfer. Figures 5.12-5.14 show vortices in the vertical planes of model M1 for all aspect ratios.

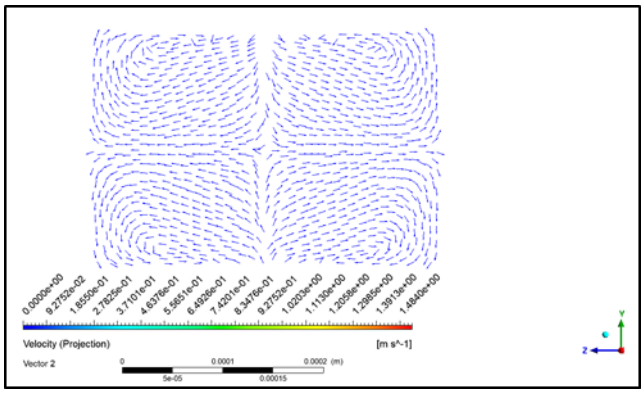

Figure 5.12 : Longitudinal vortices in the vertical plane of M1_F1_AR1.

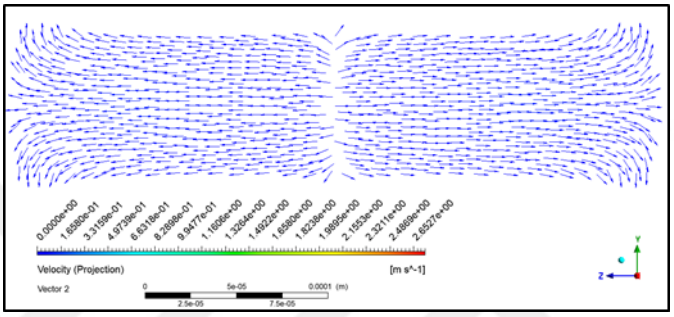

Figure 5.13 : Longitudinal vortices in the vertical plane of M1_F1_AR3.

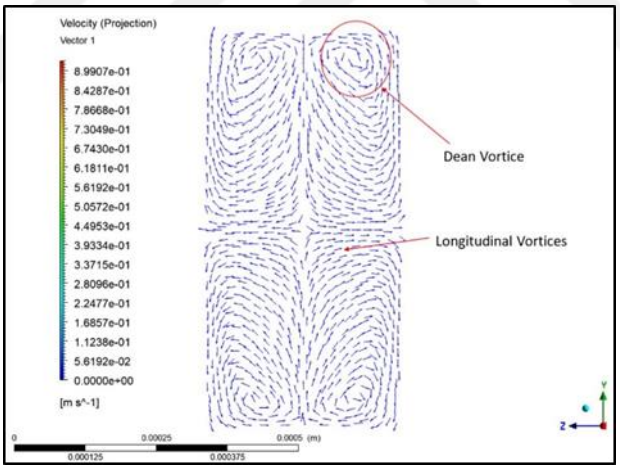

Figure 5.14 : Longitudinal vortices in the vertical plane of M1_F1_AR1/3.

Dean vortices are observed very clearly in cases which have “AR1/3” in Figure 5.14. Longitudinal vortices can have been watched at all aspect ratios.

Table 5.5 : Nu and f values with evaluation criterias for M1_AR1/3.

Case Type	Nu	f	Nu/Nu_0^*	f/f_0^*	PEC
M1_F1_AR1/3	5.54	0.077	1.01	0.970	1.015
M1_F2_AR1/3	5.49	0.076	0.99	0.947	1.017
M1_F3_AR1/3	5.10	0.074	0.94	0.888	0.978

Table 5.6 : Nu and f values with evaluation criterias for M1_AR1.

Case Type	Nu	f	Nu/Nu_0^*	f/f_0^*	PEC
M1_F1_AR1	4.26	0.0613	1.01	0.979	1.016
M1_F2_AR1	4.25	0.0617	1.01	0.974	1.019
M1_F3_AR1	4.09	0.0610	0.98	0.945	0.997

Table 5.7 : Nu and f values with evaluation criterias for M1_AR3.

Case Type	Nu	f	Nu/Nu_0^*	f/f_0^*	PEC
M1_F1_AR3	4.93	0.077	1.04	1.031	1.024
M1_F2_AR3	4.80	0.076	1.01	1.018	1.002
M1_F3_AR3	4.56	0.075	0.96	0.984	0.967

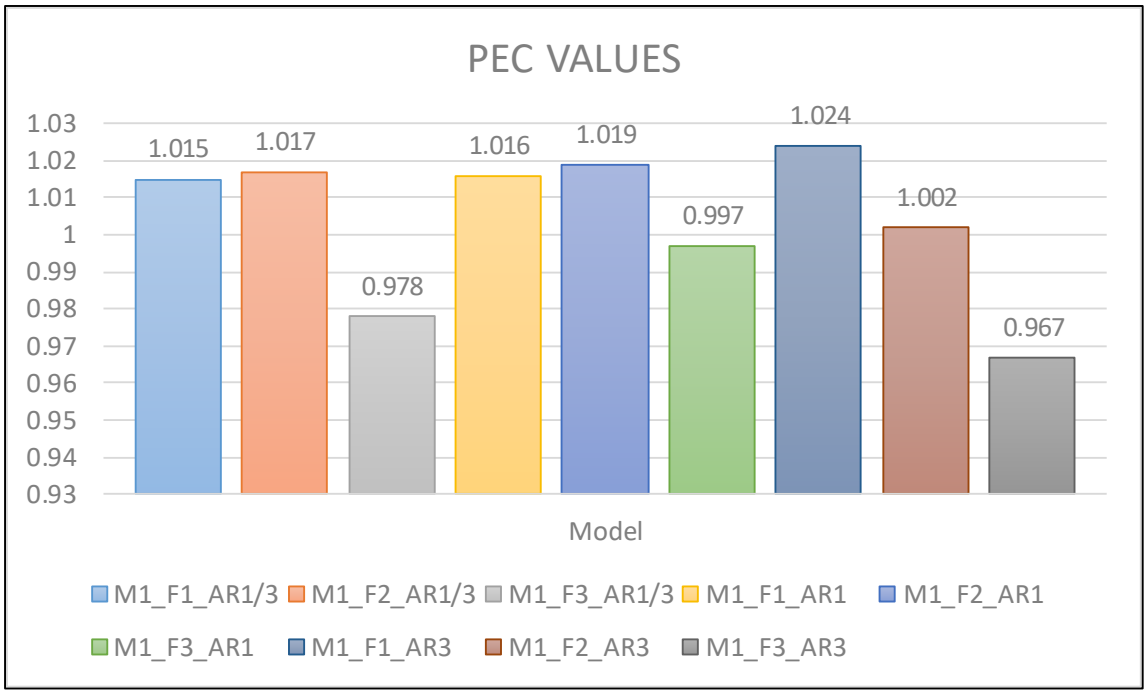

Figure 5.15 : PEC values of M1 sub-cases.

According to Tables 5.5-5.7, while keeping aspect ratio constant, increment of frequency provides decreasing in values of Nu/Nu_0^*. Recirculation zones which happens in F3 can be declared as a responsible factor about decline in Nu/Nu_0^*. In the reentrant cavities, there are stagnation points and velocity gradient is so low therefore skin friction factor decreases. Besides, recirculation zone decreases f/f_0^* significantly because of adverse pressure which decrease wall shear in the reentrant cavities.

5.2.2 Model 2

In this model, cavity and rib structures are analyzed together by using sinusoidal function. Calculated volume of one of the sub-cases is shown Figure 5.15.

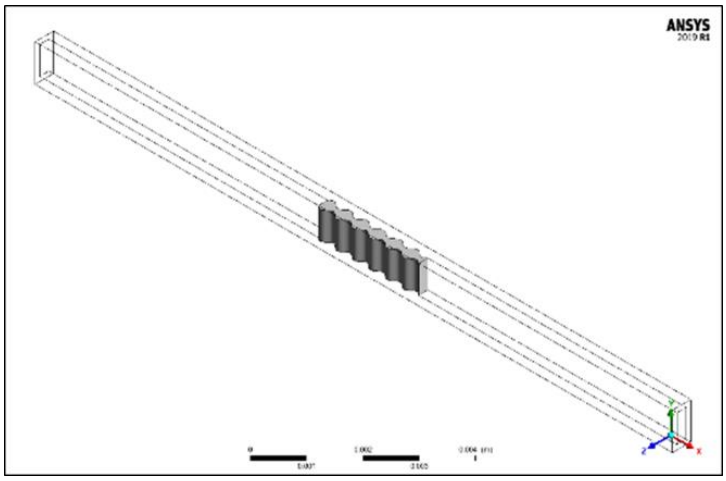

Figure 5.16 : The calculated volume of M2_F3_AR1/3.

Like Model 1, there are 9 various sub-cases in this section. For each model, central horizontal planes are taken as seen in Figure 5.16.

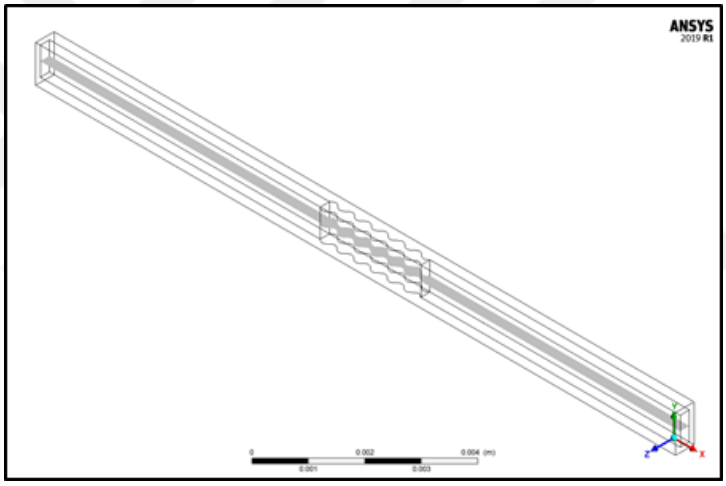

Figure 5.17 : The central horizontal plane in M2_F3_AR1/3.

For each aspect ratio, top views of fluid flow characteristics are the same. Therefore, for comparing sub cases, M2_F1_AR1, M2_F2_AR1 and M2_F3_AR1 are selected.

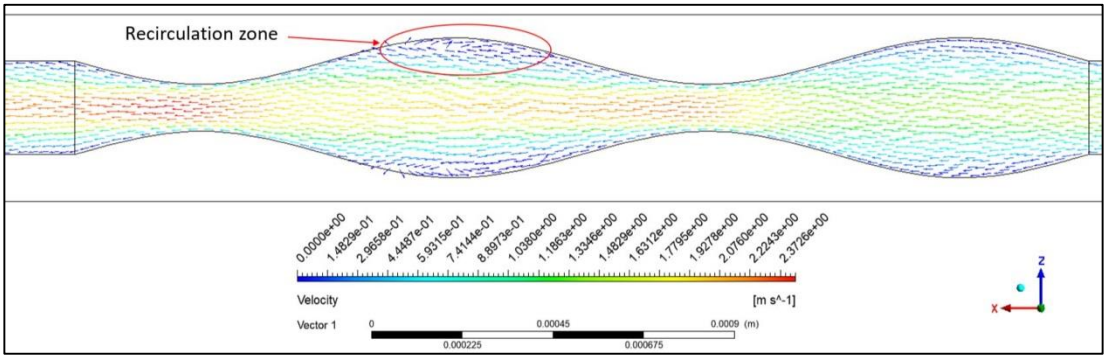

Figure 5.18 : The velocity vectors in M2_F1_AR1.

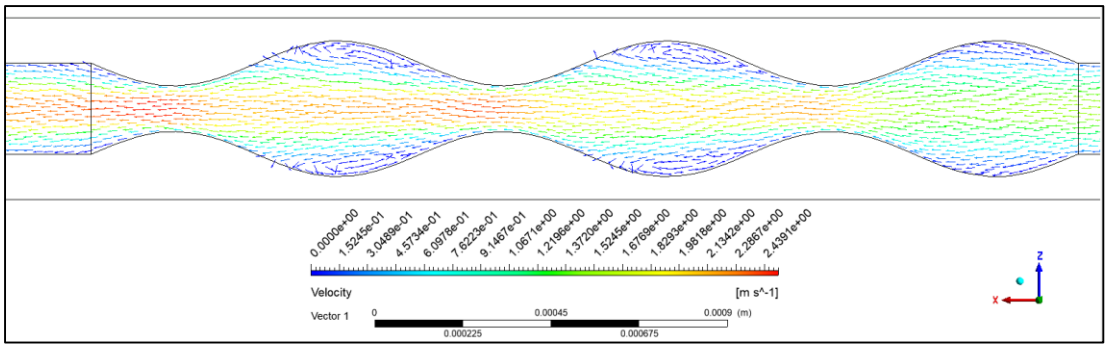

Figure 5.19 : The velocity vectors in M2_F2_AR1.

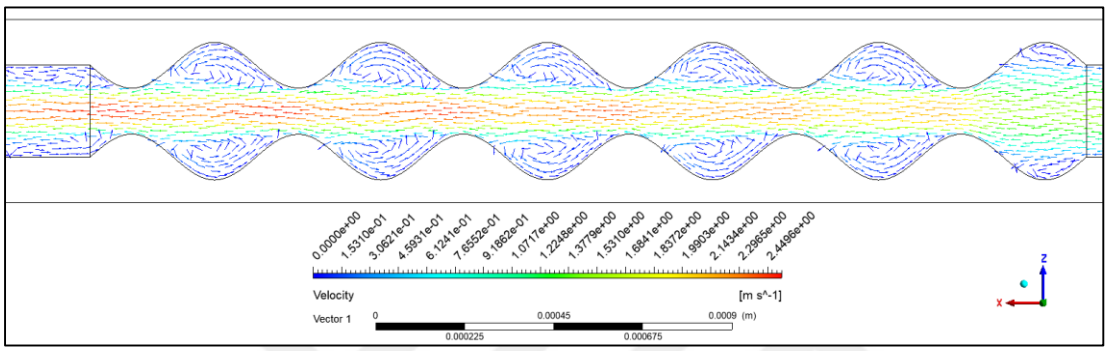

Figure 5.20 : The velocity vectors in M2_F3_AR1.

In the Figure 5.17 and Figure 5.18, first cavity does not have any recirculation zone in M2_F1_AR1 and M2_F2_AR1. However, with the increment of frequency, recirculation zone occurs at firs cavity like M2_F3_AR1 as seen Figure 5.19. Besides, vortex bubble structure can be observed after last cavity of M2_F3_AR1. In the bottlenecks, the velocity is so high and this situation cause increment in convection heat transfer.

When M2_F2_AR1 which have both no-recirculation zone and recirculation zone is tackled, jet like flows which increase heat transfer augmentation are more influential in zone which have recirculation structure as shown in Figure 5.20.

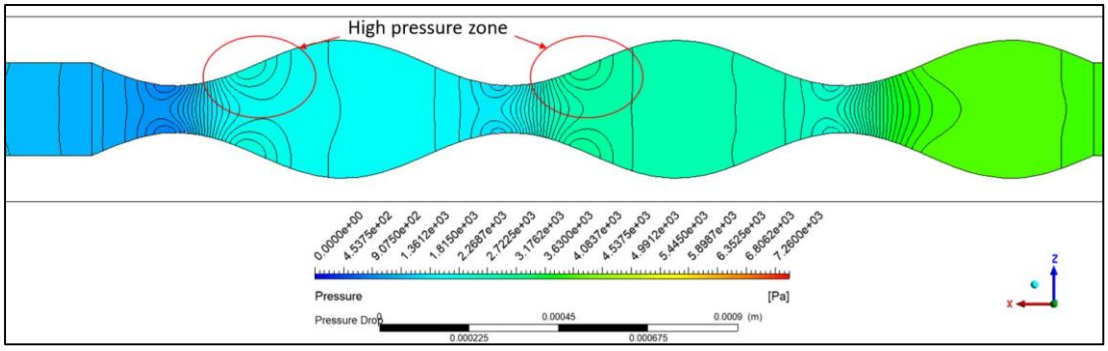

Figure 5.21 : Pressure distribution in M2_F2_AR1.

By taking vertical plane from M2_F2_AR1/3 and M2_F3_AR1/3 at their second cavity, dean vortices structure is examined in order to clarify decreasing Nu/Nu_0^* value while making frequency from F2 to F3.

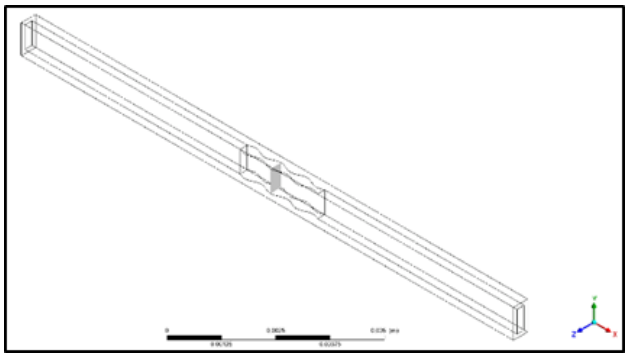

Figure 5.22 : The vertical plane in M2_F2_AR1/3.

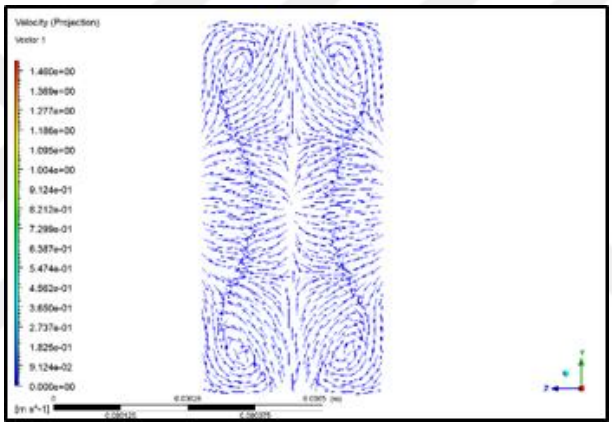

Figure 5.23 : Vortex in M2_F2_AR1/3.29

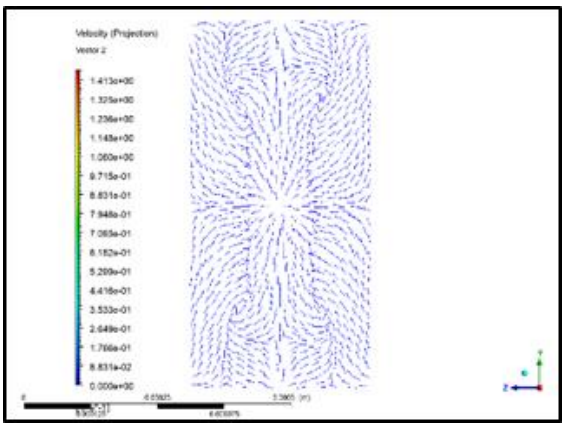

Figure 5.24 : Vortex M2_F3_AR1/3.30

In the Figures 5.21-5.23, dean vortices are more influential in M2_F2_AR1/3 than M2_F3_AR1/3 at second cavity. Therefore, mixing which enables heat transfer enhancement is more effectual in M2_F2_AR1/3.

Table 5.8 : Nu and f values with evaluation criterias for M2_AR1/3.

Case Type	Nu	f	Nu/Nu_0^*	f/f_0^*	PEC
M2_F1_AR1/3	6.47	0.118	1.16	1.540	1.003
M2_F2_AR1/3	6.71	0.119	1.20	1.556	1.038
M2_F3_AR1/3	6.06	0.117	1.11	1.439	0.981

Table 5.9 : Nu and f values with evaluation criterias for M2_AR1.

Case Type	Nu	f	Nu/Nu_0^*	f/f_0^*	PEC
M2_F1_AR1	4.98	0.081	1.15	1.021	1.021
M2_F2_AR1	5.85	0.085	1.35	1.184	1.184
M2_F3_AR1	5.22	0.083	1.22	1.089	1.089

Table 5.10 : Nu and f values with evaluation criterias for M2_AR3.

Case Type	Nu	f	Nu/Nu_0^*	f/f_0^*	PEC
M2_F1_AR3	4.51	0.074	0.91	1.104	0.881
M2_F2_AR3	4.30	0.072	0.87	1.087	0.844
M2_F3_AR3	5.08	0.073	1.03	1.095	0.995

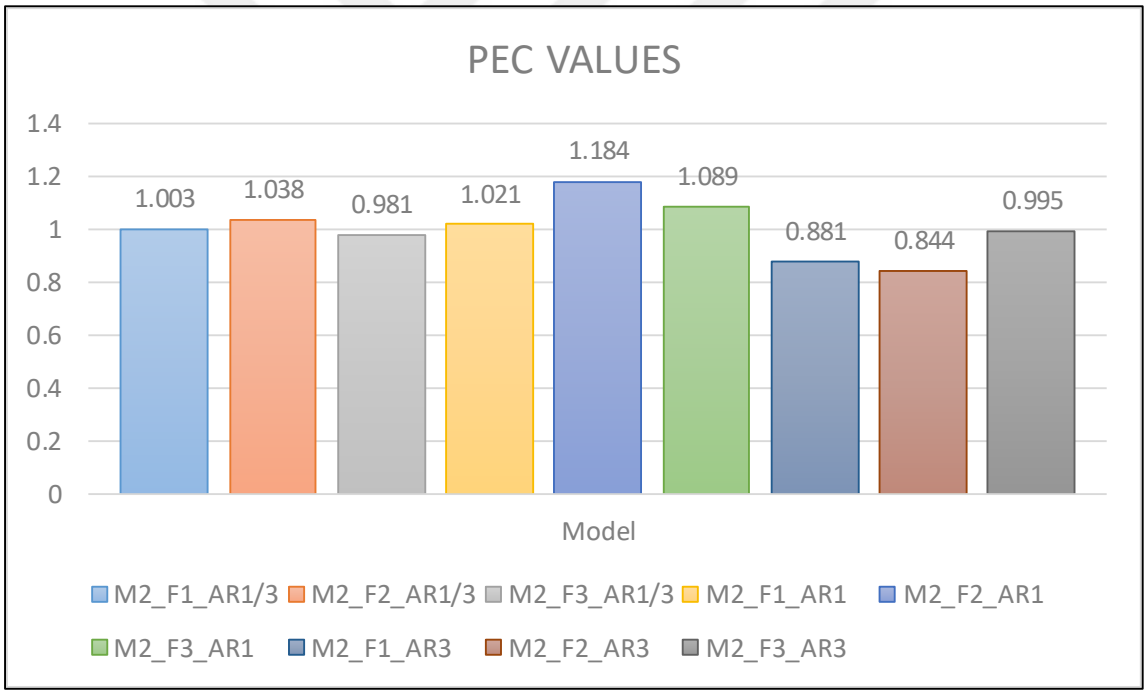

Figure 5.25 : PEC values of M2 sub-cases.

The results are obtained by using Equations, (3.13), (3.16), (3.17) and (3.18) and they are given in Tables 5.5-5.10. According to the tables, increment of frequency can not increase Nu/Nu_0^* every time, in fact this phenomenon impedes heat transfer while aspect ratio 3. Because the increasing of recirculation zone generates very slow fluid flow. The highest Nu/Nu_0^* and f/f_0^* value is countered at F2 while aspect ratio 1/3 and 1. Finally, best case for Model 2 is M2_F2_AR1.

5.2.3 Model 3

In this model, wavy channel is examined by using 9 different sub cases. The calculated region of M3_F3_AR3 which is one of them is shown in Figure 5.24.

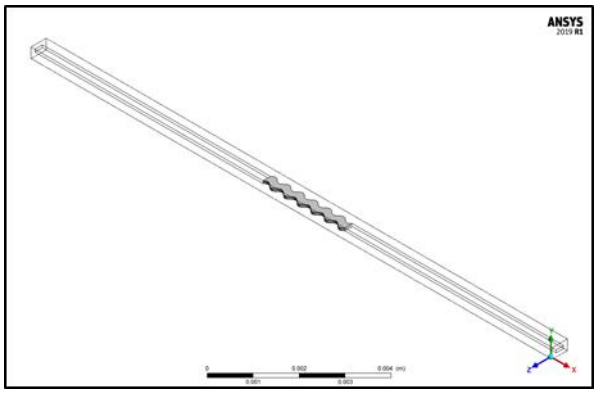

Figure 5.26 : The calculated volume of M3_F3_AR1.

For each sub-case, the center horizontal plane which is shown in Figure 5.25 is taken from models in order to observe fluid flow characteristics of sub-cases.

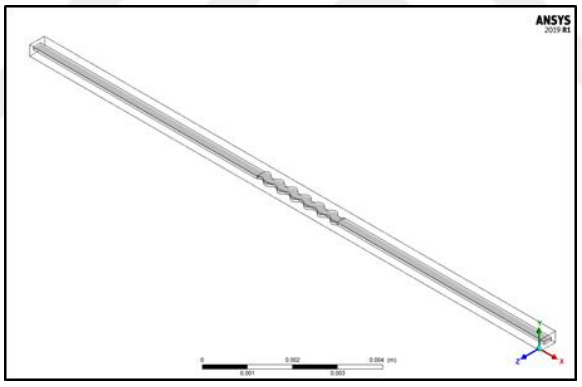

Figure 5.27 : The central horizontal plane M3_F3_AR1.

Like other models, top view of flow characteristic for each aspect ratio is same, therefore in order to examine the flow, M3_F1_AR3, M3_F2_AR3 and M3_F3_AR1/3 are chosen as seen in Figures 5.26-5.28.

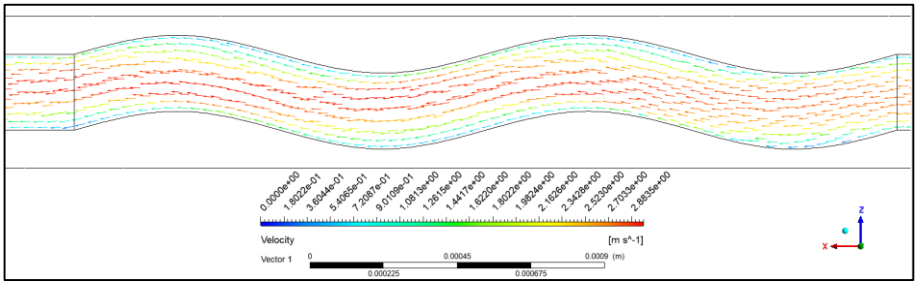

Figure 5.28 : The velocity vectors in M3_F1_AR3.

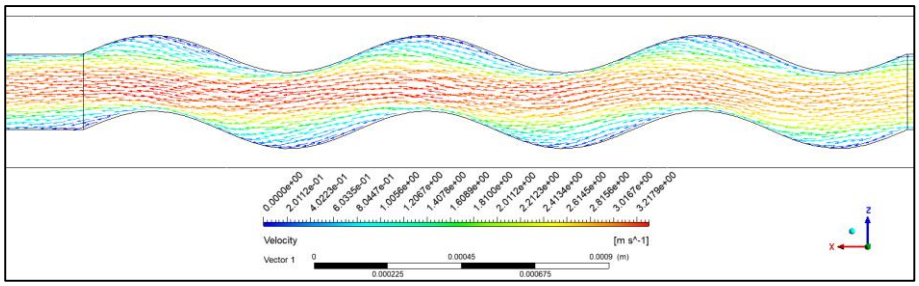

Figure 5.29 : The velocity vectors in M3_F2_AR3.

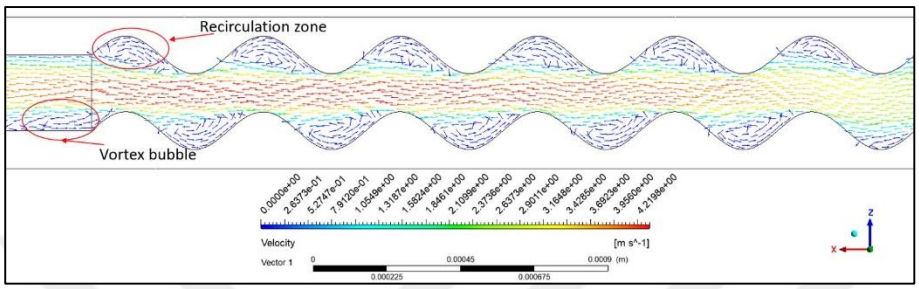

Figure 5.30 : The velocity vectors in M3_F3_AR3.

Flow which is in F1 and F2 does not have any recirculation zone as seen in Figure 5.26 and 5.27. With increasing in the frequency, velocity gradient decreasing in cavities. Therefore, this situation impedes heat transfer. Also, a vertical plane which is displayed in Figure 5.29 was taken from M3_F1_AR3 at the third cavity. Dean vortices can be observed in each sub-case. Especially, it is considered that M3_F1_AR3 have not only dean vortices which are shown in Figure 5.30 but also no recirculation zone, so Nu/Nu_o* of M3_F1_AR3 is higher than M3_F3_AR3's value. This phenomenon is obviously shown in Table 5.13.

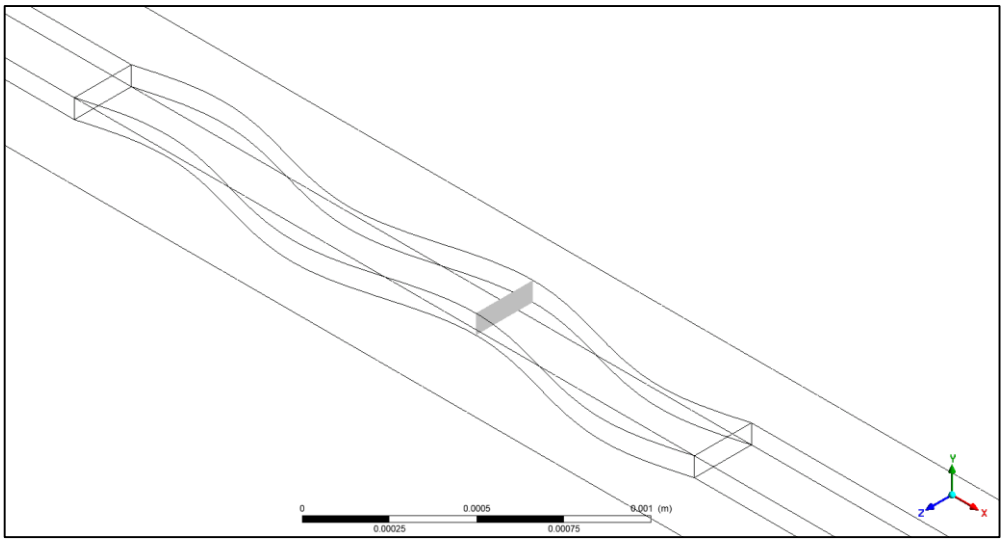

Figure 5.31 : The vertical plane in M3_F1_AR3 at third cavity.

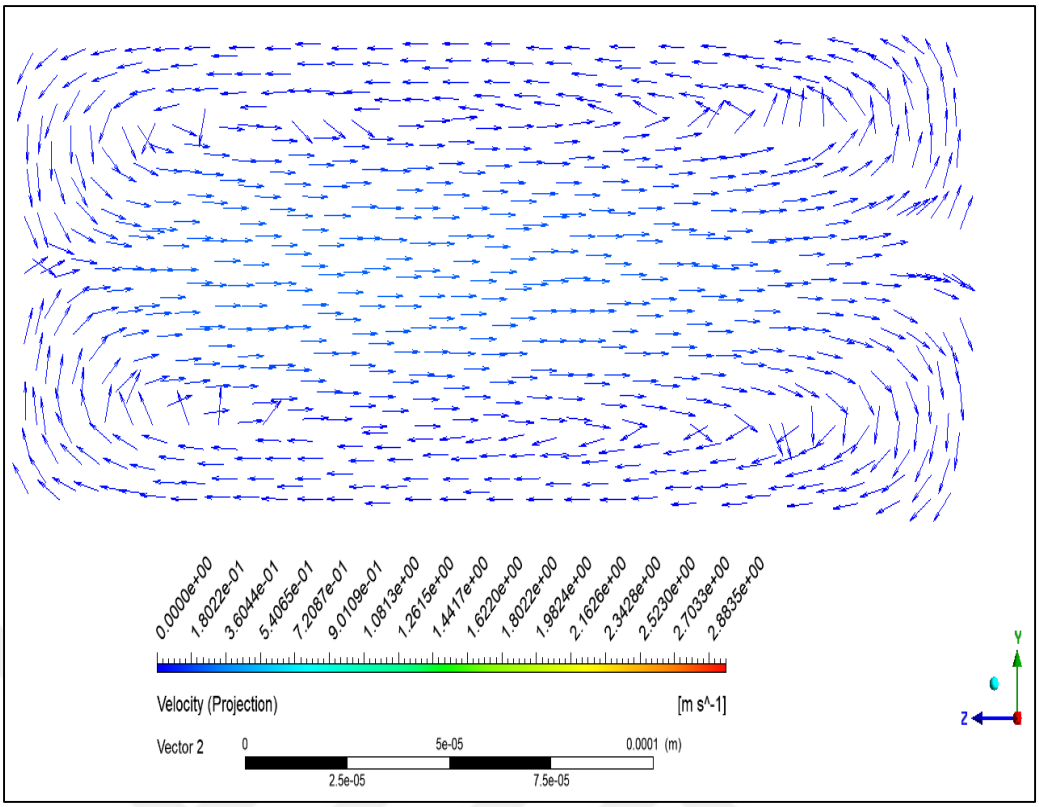

Figure 5.32 : Dean vortices in M3_F1_AR3 at third cavity.

There is a rib opposite of each cavity and this ribs disturb fluid flow and behaves as an obstacle. Therefore, with increment of frequency, number of ribs is increasing and this phenomenon raise friction factor and f/f_o* in every sub-cases in Tables 5.11-5.13.

Table 5.11 : Nu and f values with evaluation criterias for M3_AR1/3.

Case Type	Nu	f	Nu/Nu_0^*	f/f_0^*	PEC
M3_F1_AR1/3	5.65	0.080	1.02	1.051	0.999
M3_F2_AR1/3	5.67	0.084	1.02	1.085	0.992
M3_F3_AR1/3	5.65	0.109	1.04	1.330	0.941

Table 5.12 : Nu and f values with evaluaiton criterias for M3_AR1.

Case Type	Nu	f	Nu/Nu_0^*	f/f_0^*	PEC
M3_F1_AR1	4.68	0.064	1.08	1.123	1.038
M3_F2_AR1	4.70	0.069	1.09	1.185	1.026
M3_F3_AR1	4.58	0.082	1.07	1.361	0.967

Table 5.13 : Nu and f values with evaluation criterias for M3_AR3.

Case Type	Nu	f	Nu/Nu_0^*	f/f_0^*	PEC
M3_F1_AR3	5.02	0.069	1.01	1.040	0.998
M3_F2_AR3	4.84	0.070	0.98	1.058	0.958
M3_F3_AR3	4.43	0.074	0.90	1.091	0.874

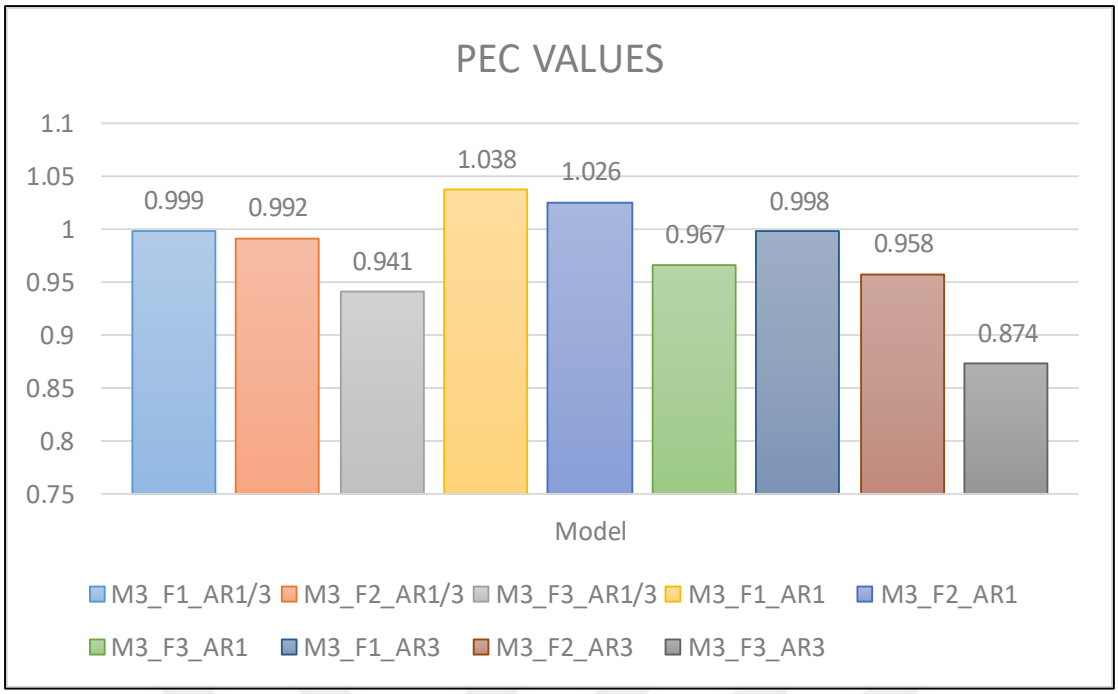

Figure 5.33 : PEC values of M3 sub-cases.

Jet like flow can be observed in only sub-cases which have F3 such as M3_F3_AR1, M3_F3_AR3 and M3_F3_AR1/3. In order to display jet like flow, the central horizontal plane is used. Each cavity has high pressure zones which are displayed in Figure 5.31.

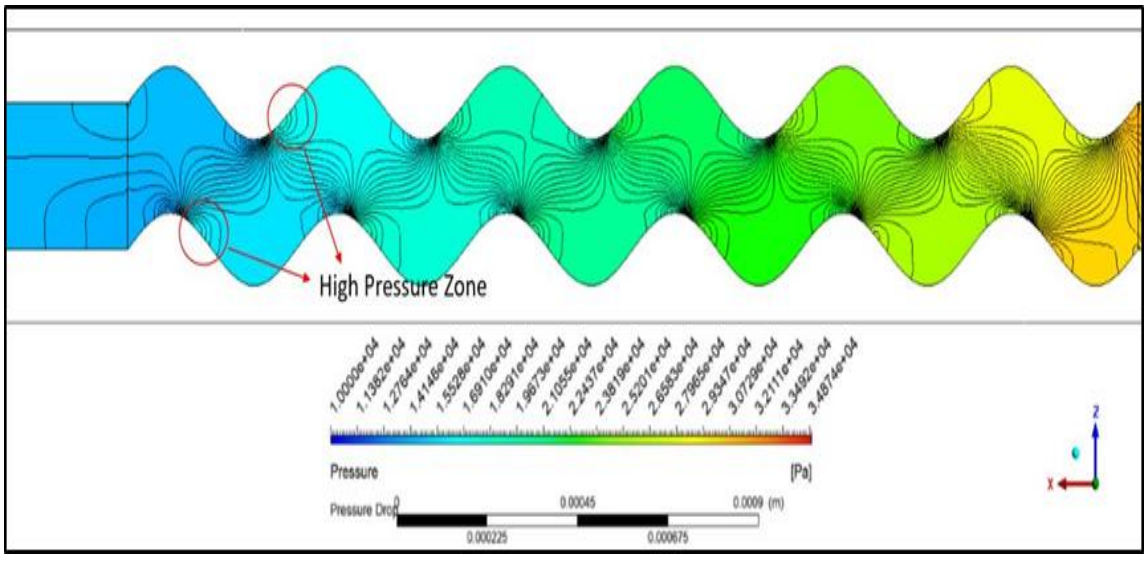

Figure 5.34 : Pressure distribution in M3_F3_AR3.

With increasing frequency, number of high pressure zones raises and this phenomenon augments heat transfer. In briefly, according to the tables, M3_F1_AR1 is the best sub-case in Model 3.

5.2.4 Model 4

In this model, influences of cavity structures which are arranged nonsymmetrical are examined with combining sinusoidal function in 9 various sub-cases. The calculated volume of one of sub-cases is shown in Figure 5.32.

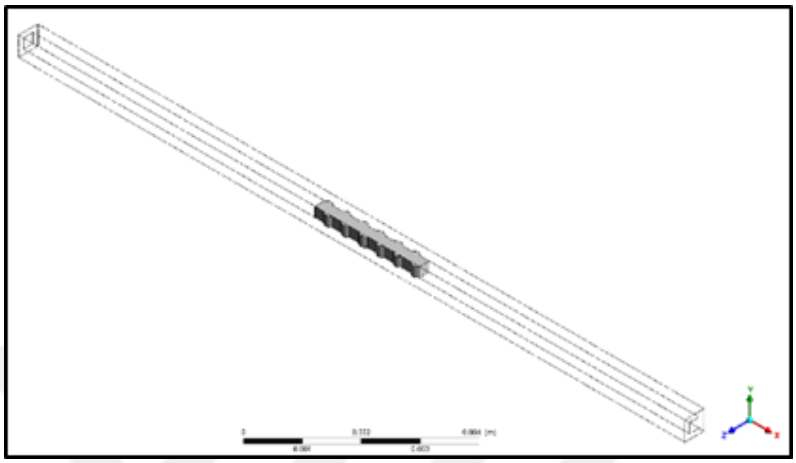

Figure 5.35 : The calculated volume M4_F3_AR1.

In order to observe the flow characteristic in microchannels, a central horizontal plane which is shown in Figure 5.33 is taken from sub-cases which are M4_F1_AR1, M4_F2_AR3 and M4_F3_AR1/3.

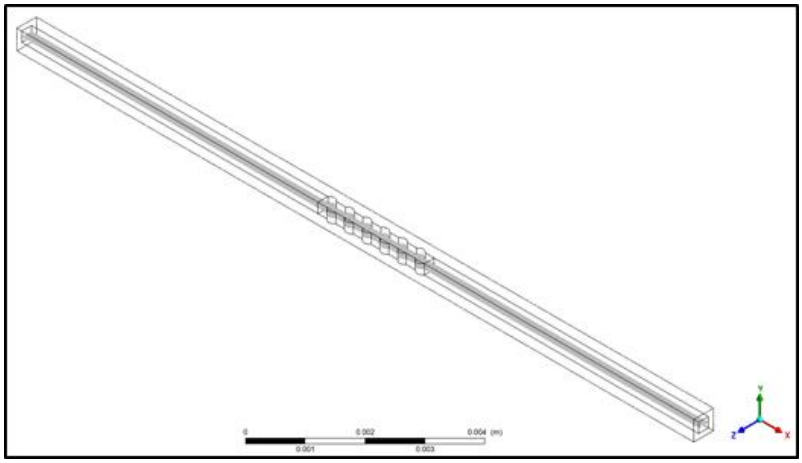

Figure 5.36 : The central horizontal plane of M4_F3_AR1.

In this model, there are sudden expansion regions which make velocity too low like Model 1. Velocity gradient is so low near the cavities, this phenomena decreases wall shear. Besides, especially this situation indirectly reduces friction factor significantly.

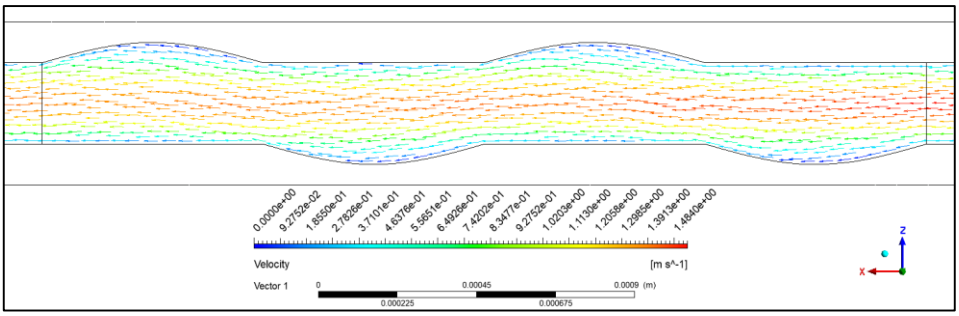

Figure 5.37 : Velocity vectors of M4_F2_AR1.

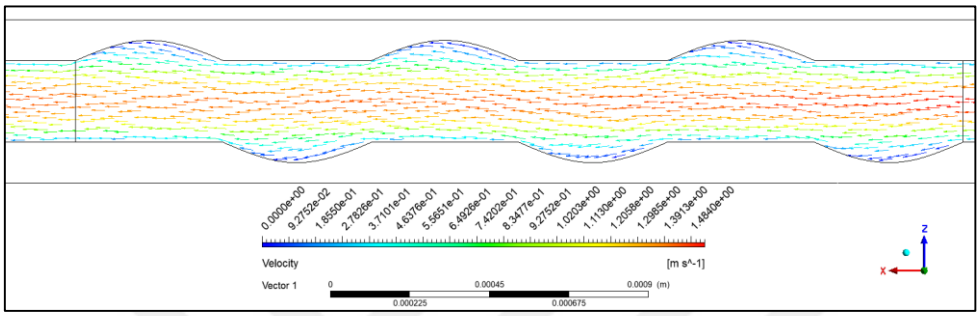

Figure 5.38 : Velocity vectors of M4_F2_AR1.

For F1 and F2, recirculation zone can not be observed in each cavity as shown in Figures 5.34 and 5.35. However, recirculation zones are appeared in every cavity region of M4_F3_AR1 like M1_F3_AR1 and other sub-cases which have F3. This phenomenon can be observed in Figure 5.36.

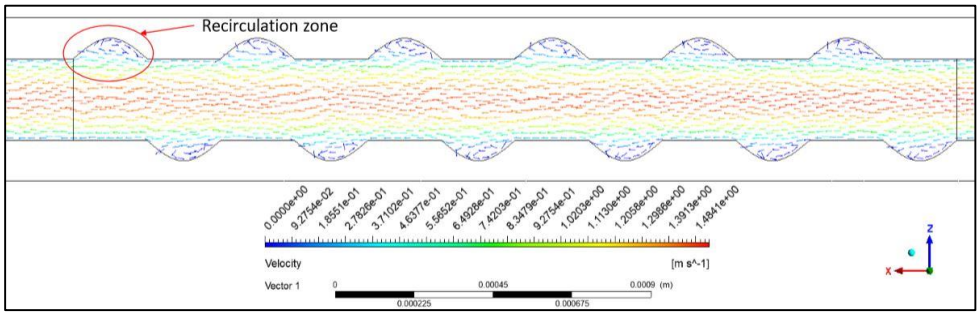

Figure 5.39 : Velocity vectors of M4_F2_AR1.

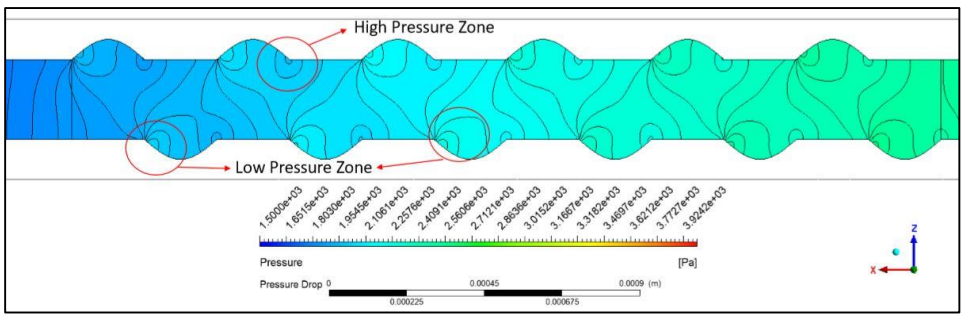

Figure 5.40 : Pressure distribution in M4_F3_AR1.

This phenomena, for this model, increasing in frequency induce significant decreasement in Nusselt Number and Nu/Nu_0^* of sub-cases. This situation is shown in Table 5.15. The pressure drops step by step throughout the microchannel. Furthermore, there are jet like flows which generate high pressure zones which are shown in Figure 5.37 in cavities. The results are given in Tables 5.14-5.15. As a result, M4_F1_AR3 which have also the highest Nu/Nu_o* is the best sub-case for Model 4 according to its PEC value.

Table 5.14 : Nu and f values with evaluation criterias for M4_AR1/3.

Case Type	Nu	f	Nu/Nu_0^*	f/f_0^*	PEC
M4_F1_AR1/3	5.40	0.072	0.98	0.911	1.009
M4_F2_AR1/3	5.37	0.072	0.98	0.901	1.010
M4_F3_AR1/3	5.05	0.073	0.93	0.875	0.973

Table 5.15 : Nu and f values with evaluation criterias for M4_AR1.

Case Type	Nu	f	Nu/Nu_0^*	f/f_0^*	PEC
M4_F1_AR1	4.22	0.059	1.000	0.944	1.019
M4_F2_AR1	4.19	0.059	0.99	0.943	1.013
M4_F3_AR1	4.05	0.060	0.97	0.935	0.991

Table 5.16 : Nu and f_o values with evaluation criterias for M4_AR3.

Case Type	Nu	f	Nu/Nu_0^*	f/f_0^*	PEC
M4_F1_AR3	4.98	0.076	1.04	1.015	1.039
M4_F2_AR3	4.79	0.075	1.01	1.004	1.001
M4_F3_AR3	4.56	0.074	0.96	0.990	0.966

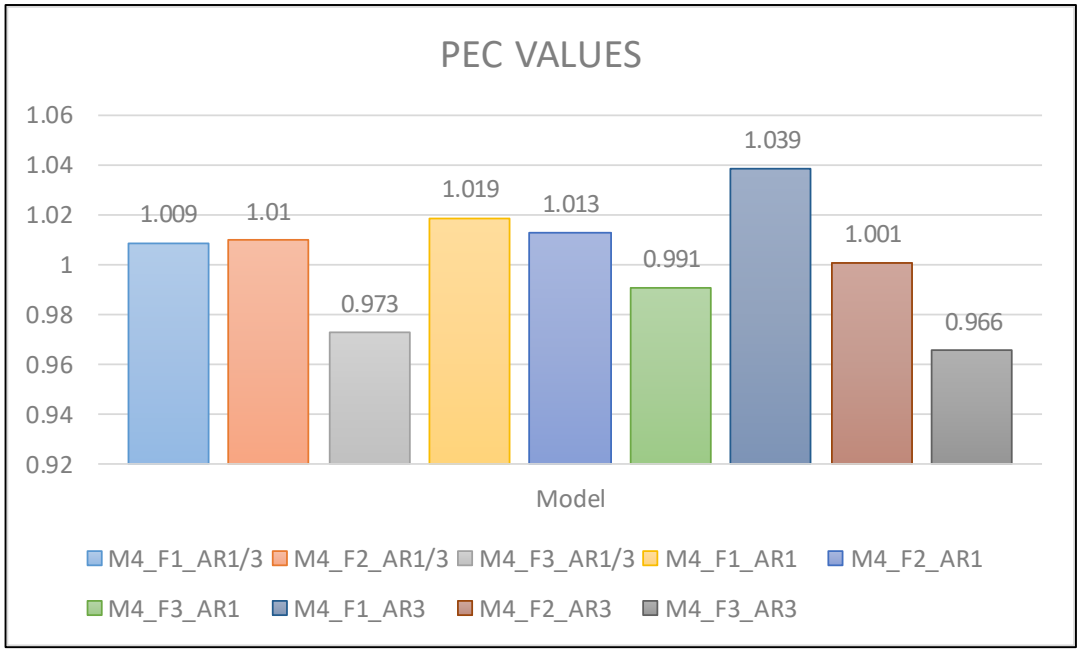

Figure 5.41 : PEC values of M4 sub-cases.

5.2.5 Model 5

In this model, influences of rib structure which is combined with sinusoidal wave are examined. This model can be considered opposite of Model 4. There are only sudden constriction zones unlike Model 1 and Model 4 which have only sudden expansion regions. The calculated volume and the central horizontal plane of Model 5 are displayed in Figures 5.38 and 5.39.

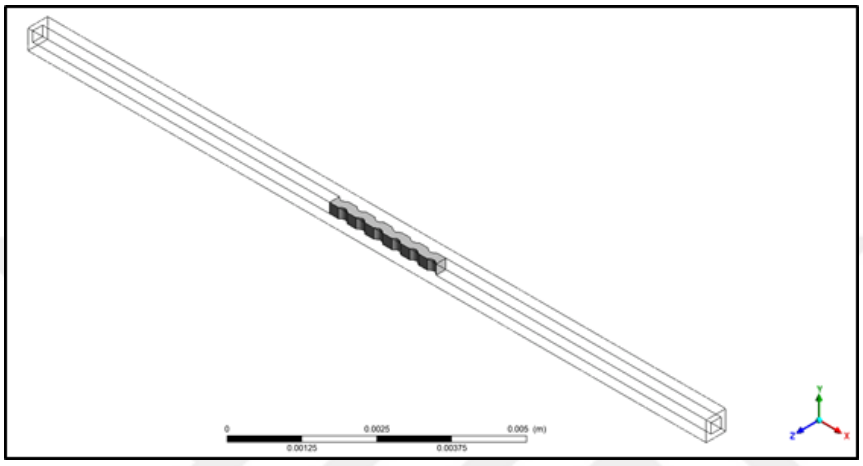

Figure 5.42 : The calculated volume in M5_F3_AR1.

Owing to that top views of sub-cases which have different aspect ratios and same frequency are similar, analyzing one aspect ratio is enough.

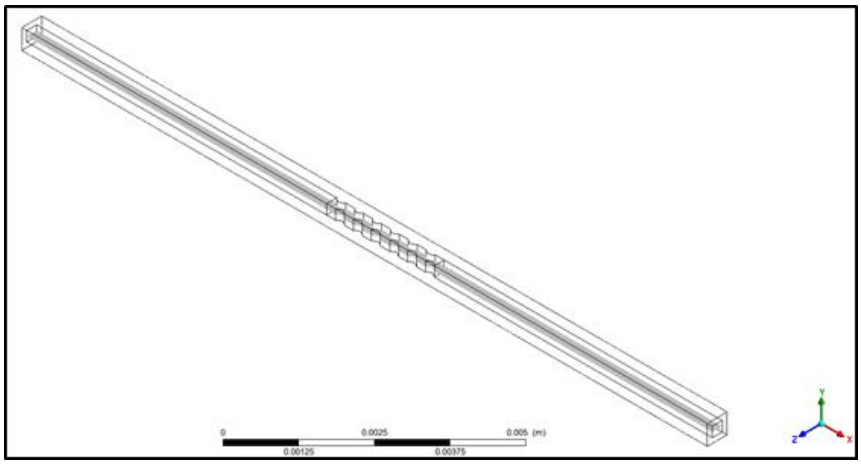

Figure 5.43 : The central horizontal plane of M5_F3_AR1.

Therefore, in order to comprehend the fluid flow characteristic in the calculated volume, a central horizontal plane is taken from M5_F1_AR1, M5_F2_AR1 and M5_F3_AR1.

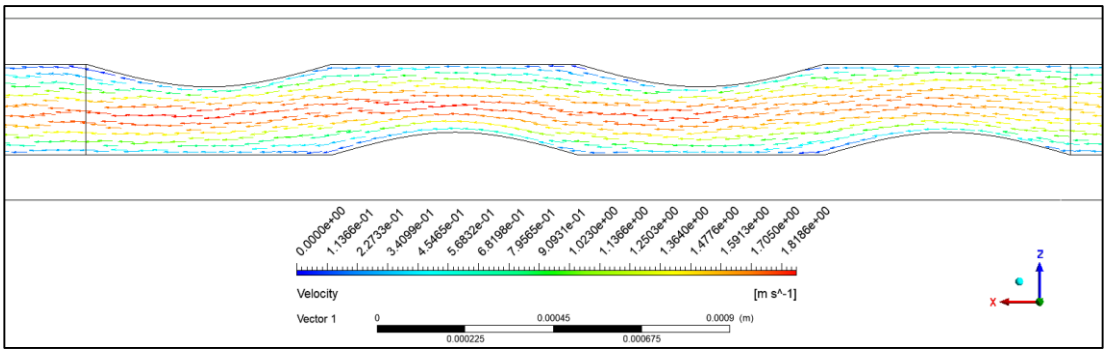

Figure 5.44 : Velocity vectors in M5_F1_AR1.

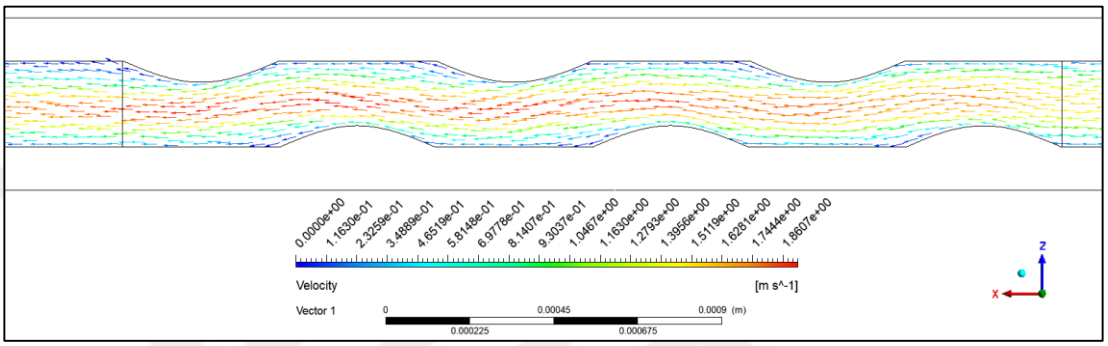

Figure 5.45 : Velocity vectors in M5_F2_AR1.

Recirculation zone and vortex bubble structures do not occur in sub-cases which have F1 and F2. Figures 5.40 and 5.41 can be given as examples for this situation. However, with the increasing of frequency, vortex bubble and recirculation zone structure can be observed in sub-cases which have F3. These phenomena are displayed in Figure 5.42.

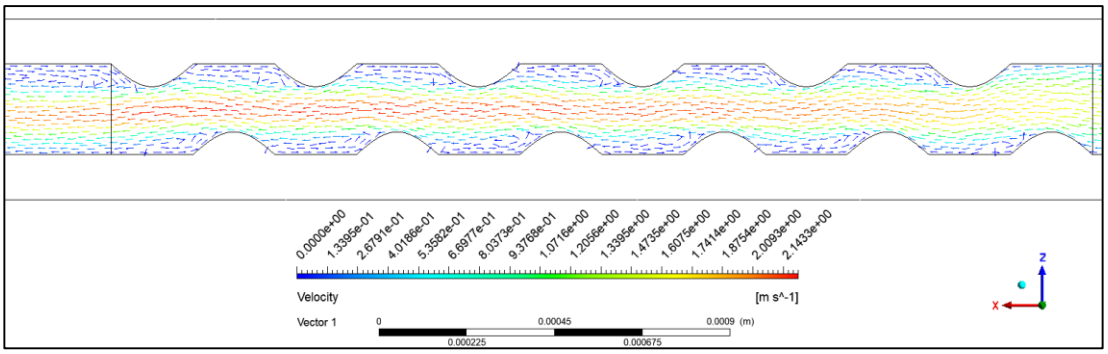

Figure 5.46 : Velocity vector in M5_F3_AR1.

In the inside of the microchannel, low pressure zone is observed at the point where fluid separates. Besides, there are high pressure zones because of jet like flows. These phenomena are shown in Figure 5.40.

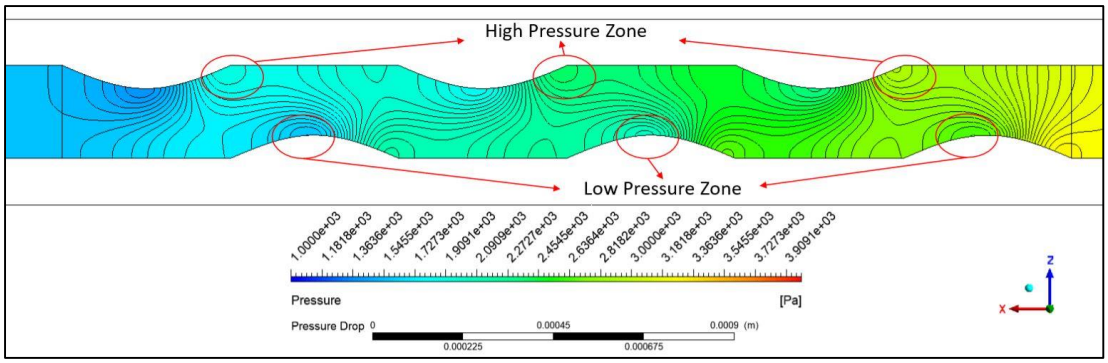

Figure 5.47 : Pressure distribution in M5_F2_AR1.

Also, a vertical plane which is shown in Figure 5.43 was taken from third rib in M5_F1_AR1.

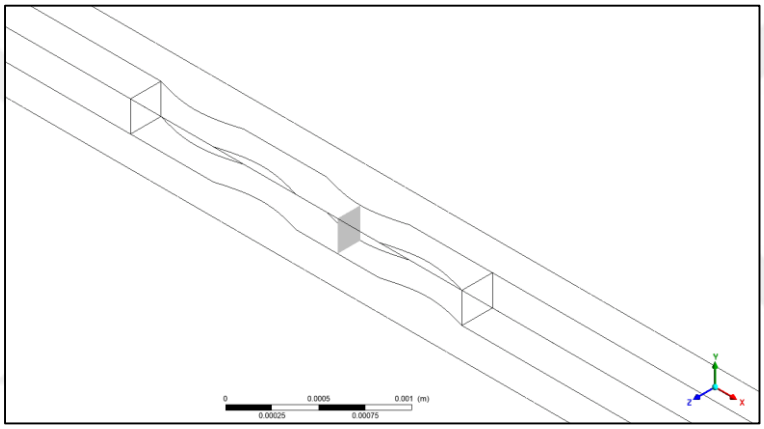

Figure 5.48 : A vertical plane in M5_F1_AR1 at third rib.

Because of curly structure, small dean vortices can be observed with longitudinal vortices at the vertical plane. This phenome can be displayed in Figure 5.44. This situation increase mixing and therefore heat transfer enhancement increases.

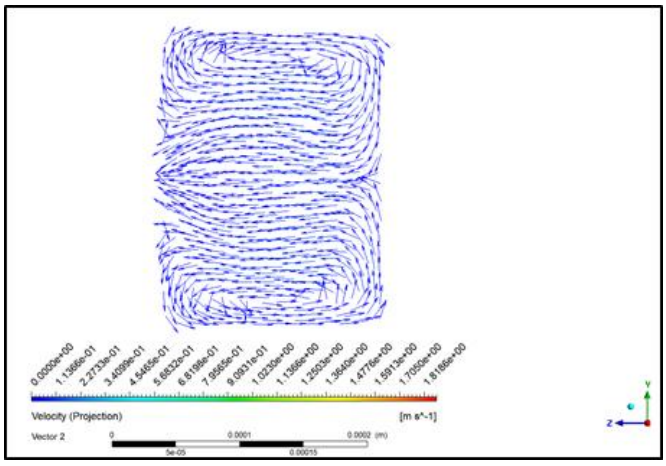

Figure 5.49 : Longitudinal vortices at the vertical plane in M5_F1_AR1.

Ribs behave as an obstacle for fluid flow. Therefore, with the increment of frequency, friction factor and f/f_0^* values increase with significantly as shown in Tables 5.17-5.19.

Table 5.17 : Nu and f values with evaluation criterias for M5_AR1/3.

Case Type	Nu	f	Nu/Nu_0^*	f/f_0^*	PEC
M5_F1_AR1/3	5.77	0.812	1.02	1.106	0.985
M5_F2_AR1/3	5.71	0.814	1.01	1.102	0.978
M5_F3_AR1/3	5.32	0.861	0.95	1.182	0.901

As a result, increment in frequency increases Nu value for AR1/3 and AR1. However, for AR3, decreasement in frequency increases Nu value. According to PEC values, none of else can be recommended. On the other hand, modifications are useful for increasing Nu/Nu_o* for some sub-cases.

Table 5.18 : Nu and f values with evaluation criterias for M5_AR1.

Case Type	Nu	f	Nu/Nu_0^*	f/f_0^*	PEC
M5_F1_AR1	4.53	0.059	1.02	1.116	0.980
M5_F2_AR1	4.54	0.061	1.02	1.144	0.974
M5_F3_AR1	4.60	0.066	1.04	1.214	0.976

Table 5.19 : Nu and f values with evaluation criterias for M5_AR3.

Case Type	Nu	f	Nu/Nu_0^*	f/f_0^*	PEC
M5_F1_AR3	4.86	0.059	0.94	1.007	0.940
M5_F2_AR3	4.83	0.060	0.94	1.021	0.929
M5_F3_AR3	4.60	0.061	0.89	1.023	0.888

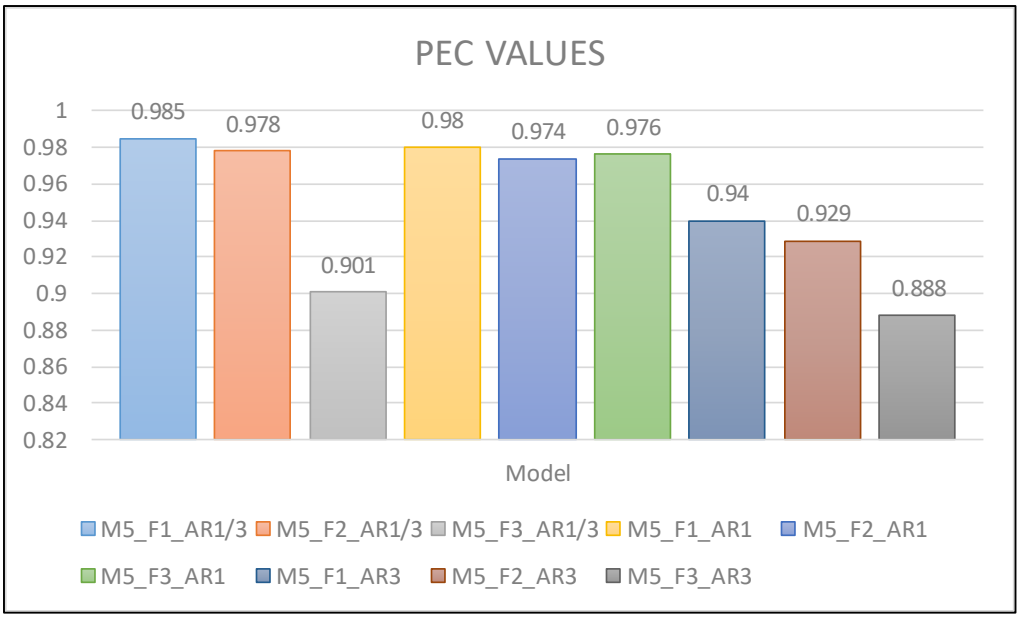

Figure 5.50 : PEC values of M5 sub-cases.

6. CONCLUSIONS AND RECOMMENDATIONS

There is a gradually expanding requirement for thermal management in order to remove heat flux which can demolish electronic devices. In the present study basic comprehension understanding of the influences which are occurred because of ribs and cavities for incompressible fluid flow in microchannel heat sinks has been discussed. Different influences were investigated in various designed 5 models. Shortly, Model 1 has only the reentrant cavities, therefore boundary layer interruption was targeted phenomena. Because of the reentrant cavities, sudden expansions occur and velocity gradients dramatically reduce, so values of wall shear which is related to fanning friction decrease significantly. In spite of Model 1, there are not only cavities but also ribs in Model 2. By virtue of these structures, sudden expansion and contraction ensue together therefore increment in pressure drop and fanning friction factor were expected. Model 3, has wavy wall structure also cross-section is constant along the channel. In this model, the reentrant cavities and ribs were arranged in sync. Unlike Model 1, the reentrant cavities are collocated unsymmetrically in Model 4. Finally, Model 5 has only the reentrant ribs which are arranged unsymmetrically. Therefore, these ribs behave in the flow area as obstacles which increase fanning friction factor.

Throughout the master thesis, a special code was used in order to categorize sub-cases and increase comprehensibility. Each model is symbolized as M1, M2, M3, M4 and M5. Besides, there are 3 different sinusoidal function which have 3 various frequencies, so these functions are denoted as F1, F2 and F3. Moreover, in order to indicate 3 diverse aspect ratios, AR1/3, AR1 and AR3 were used. For example, when M2_F3_AR1 is declared, that the sub-case has features of Model 2, third function and aspect ratio which is 1 must be understood

Various flow characteristics were observed in each sub-cases. One of them was recirculation zones which make velocity gradient low. Especially, recirculation zones occurred in cavity and separation points. Velocity gradient in these region is too low and this situation causes low Reynolds number. However, while looking at vertical

planes which were taken from sub-cases, longitudinal and Dean vortices could be observed. This vortex provides mixing of fluid between cool and hot part. This phenomenon induces increment of convection heat transfer, so increasing in Nusselt number occurs. According to the results, generally sub-cases which have the lowest aspect ratio has the highest Nusselt number, but it is not enough comparing. For comparing, x^+ values must be calculated and known. Because, Nu values are valid when x^+ is declared for thermal entry length problem. Moreover, foremost evaluation criterion is PEC number. Because PEC number includes Nusselt number ratio (Nu/Nu_0^*) and friction factor ratio (f/f_0^*). That increment in frequency can not be beneficial for each sub-cases on heat transfer enhancement. For instances, in M1 sub cases, Nu/Nu_0^* values decrease with frequency is increased. However, in some M2 sub cases, rising frequency from F1 to F2 provides increment in heat transfer enhancement. Besides, PEC values significantly decreased with rising in frequency from F1 to F3. Therefore, there is no linear by linear association between PEC values and geometric alterations every time. For these sub-cases, generalization would not be correct always. Therefore, each model should be examined separately.

As as result, sub-case which have the highest PEC number is M2_F2_AR1. Therefore, M2_F2_AR1 is recommended for using cooling applications.

REFERENCES

Abdul Hasis, F. Bin, Mithun Krishna, P. M., Aravind, G. P., Deepu, M., & Shine, S. R. (2018). Thermo hydraulic performance analysis of twisted sinusoidal wavy microchannels. *International Journal of Thermal Sciences*, *128* (May 2017), 124–136. https://doi.org/10.1016/j.ijthermalsci.2018.02.018

Ahmed, H. E., & Ahmed, M. I. (2015). Optimum thermal design of triangular, trapezoidal and rectangular grooved microchannel heat sinks. *International Communications in Heat and Mass Transfer*, *66*, 47–57. https://doi.org/10.1016/j.icheatmasstransfer.2015.05.009

Colin, S. (2013). Single-Phase Gas Flow in Microchannels. *Heat Transfer and Fluid Flow in Minichannels and Microchannels*, 11–102. https://doi.org/10.1016/B978-0-08-098346-2.00002-8

Fiebig, M. (1995). Embedded vortices in internal flow: heat transfer and pressure loss enhancement. *International Journal of Heat and Fluid Flow*, *16*(5), 376–388. https://doi.org/10.1016/0142-727X(95)00043-P

Ghani, I. A., Kamaruzaman, N., & Sidik, N. A. C. (2017a). Heat transfer augmentation in a microchannel heat sink with sinusoidal cavities and rectangular ribs. *International Journal of Heat and Mass Transfer*, *108*, 1969–1981. https://doi.org/10.1016/j.ijheatmasstransfer.2017.01.046

Ghani, I. A., Sidik, N. A. C., & Kamaruzaman, N. (2017b). Hydrothermal performance of microchannel heat sink: The effect of channel design. *International Journal of Heat and Mass Transfer*, *107*, 21–44. https://doi.org/10.1016/j.ijheatmasstransfer.2016.11.031

Hong, F., & Cheng, P. (2009). Three dimensional numerical analyses and optimization of offset strip-fin microchannel heat sinks. *International Communications in Heat and Mass Transfer*, *36*(7), 651–656. https://doi.org/10.1016/j.icheatmasstransfer.2009.02.015

Kandlikar, S. G., Grande, W. J., Lee, P. S., Garimella, S. V., Liu, D., Tuckerman, D. B., … Mahulikar, S. P. (2002). Ts toc. *International Journal of Heat and Mass Transfer*, *48*(9), 1688–1704. https://doi.org/10.1016/j.ijheatmasstransfer.2004.11.019

Kandlikar, S. G., Garimella, S., Li, D., Colin, S., & King, M. R. (2006). *Heat Transfer and Fluid Flow in Minichannels and Microhannels*. https://doi.org/10.1016/B978-0-08-044527-4.X5000-2

Kestin, J., Sokolov, M., Wakeham, W.A. (1978). Viscosity of liquid water in the range -8 C to 150 C, J. Phys. and Chem. Ref. Data 7 (941) 941–948. http://dx.doi.org/10.1063/1.555581

Kumar, P. (2019). Numerical investigation of fluid flow and heat transfer in trapezoidal microchannel with groove structure. *International Journal of Thermal Sciences*, *136*(January 2018), 33–43. https://doi.org/10.1016/j.ijthermalsci.2018.10.006

Mohammed, H. A., Gunnasegaran, P., & Shuaib, N. H. (2011). Numerical simulation of heat transfer enhancement in wavy microchannel heat sink. *International Communications in Heat and Mass Transfer*, *38*(1), 63–68. https://doi.org/10.1016/j.icheatmasstransfer.2010.09.012

Sui, Y., Lee, P. S., & Teo, C. J. (2011). An experimental study of flow friction and heat transfer in wavy microchannels with rectangular cross section. *International Journal of Thermal Sciences*, *50*(12), 2473–2482. https://doi.org/10.1016/j.ijthermalsci.2011.06.017

Sui, Y., Teo, C. J., & Lee, P. S. (2012). Direct numerical simulation of fluid flow and heat transfer in periodic wavy channels with rectangular cross-sections. *International Journal of Heat and Mass Transfer*, *55*(1–3), 73–88. https://doi.org/10.1016/j.ijheatmasstransfer.2011.08.041

Tuckerman, D. B., & Pease, R. F. W. (1981). High-performance heat sinking for VLSI. *IEEE Electron Device Letters*, *2*(5), 126–129. https://doi.org/10.1109/EDL.1981.25367

Tullius, J. F., Vajtai, R., & Bayazitoglu, Y. (2011). A review of cooling in microchannels. *Heat Transfer Engineering*, *32*(7–8), 527–541. https://doi.org/10.1080/01457632.2010.506390

Xia, G., Chai, L., Zhou, M., & Wang, H. (2011). Effects of structural parameters on fluid flow and heat transfer in a microchannel with aligned fan-shaped reentrant cavities. *International Journal of Thermal Sciences*, *50*(3), 411–419. https://doi.org/10.1016/j.ijthermalsci.2010.08.009

Xia, G., Zhai, Y., & Cui, Z. (2013). Numerical investigation of thermal enhancement in a micro heat sink with fan-shaped reentrant cavities and internal ribs. *Applied Thermal Engineering*, *58*(1–2), 52–60. https://doi.org/10.1016/j.applthermaleng.2013.04.005

Wang, H., Chen, Z., & Gao, J. (2016). Influence of geometric parameters on flow and heat transfer performance of micro-channel heat sinks. *Applied Thermal Engineering*, *107*, 870–879. https://doi.org/10.1016/j.applthermaleng.2016.07.039

Zheng, Z., Fletcher, D. F., & Haynes, B. S. (2014). Transient laminar heat transfer simulations in periodic zigzag channels. *International Journal of Heat and Mass Transfer*, *71*, 758–768. https://doi.org/10.1016/j.ijheatmasstransfer.2013.12.056

APPENDICES

APPENDIX A: Mesh Figures in M2_F3_AR1

APPENDIX B: User define function for dynamic viscosity

APPENDIX A

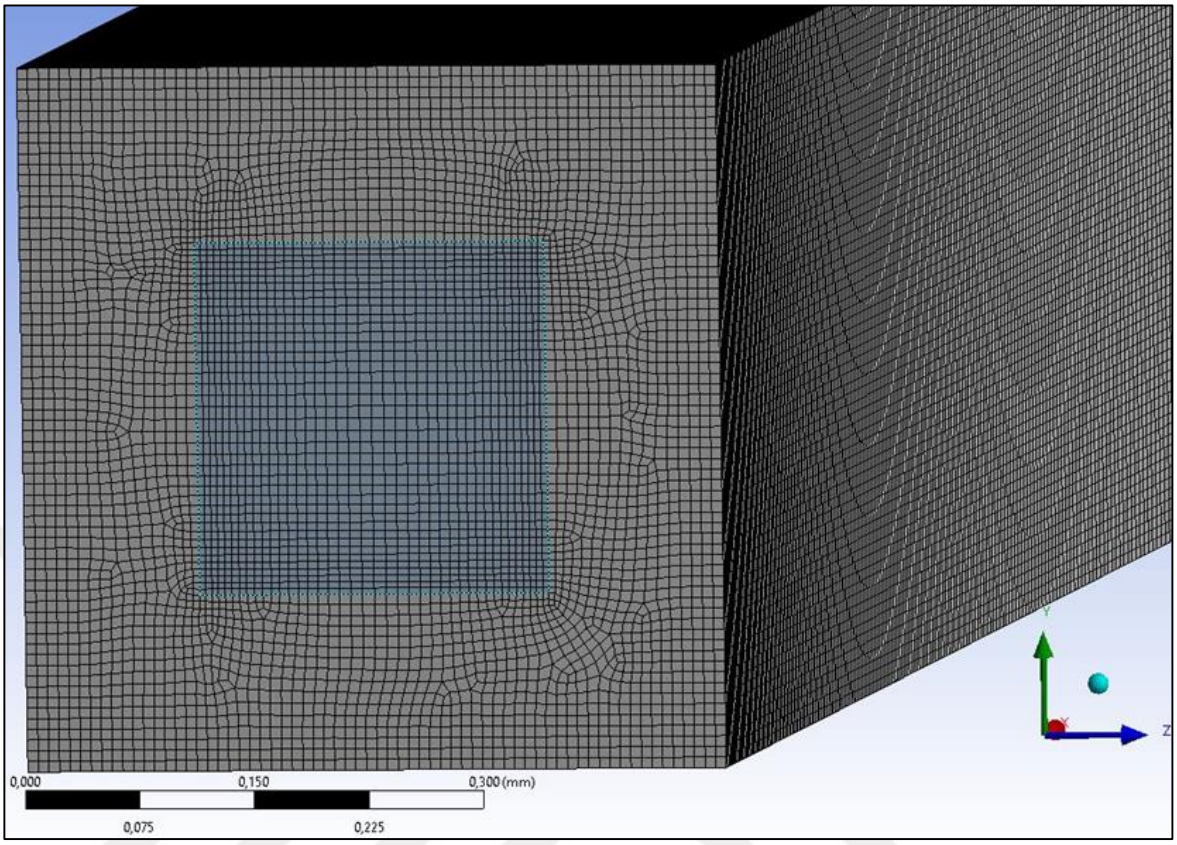

Figure A.1 : Solid region of Mesh_1 in M2_F3_AR1.

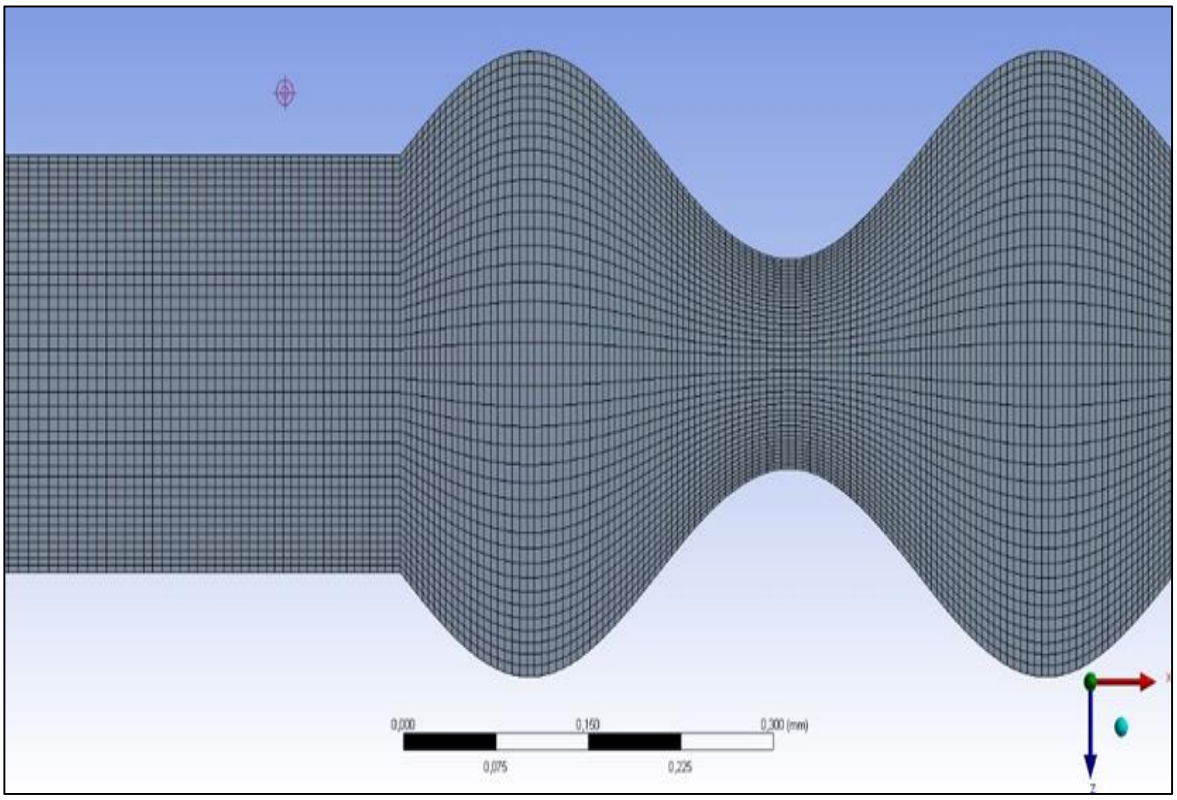

Figure A.2 : Fluid region of Mesh_1 in M2_F3_AR1.

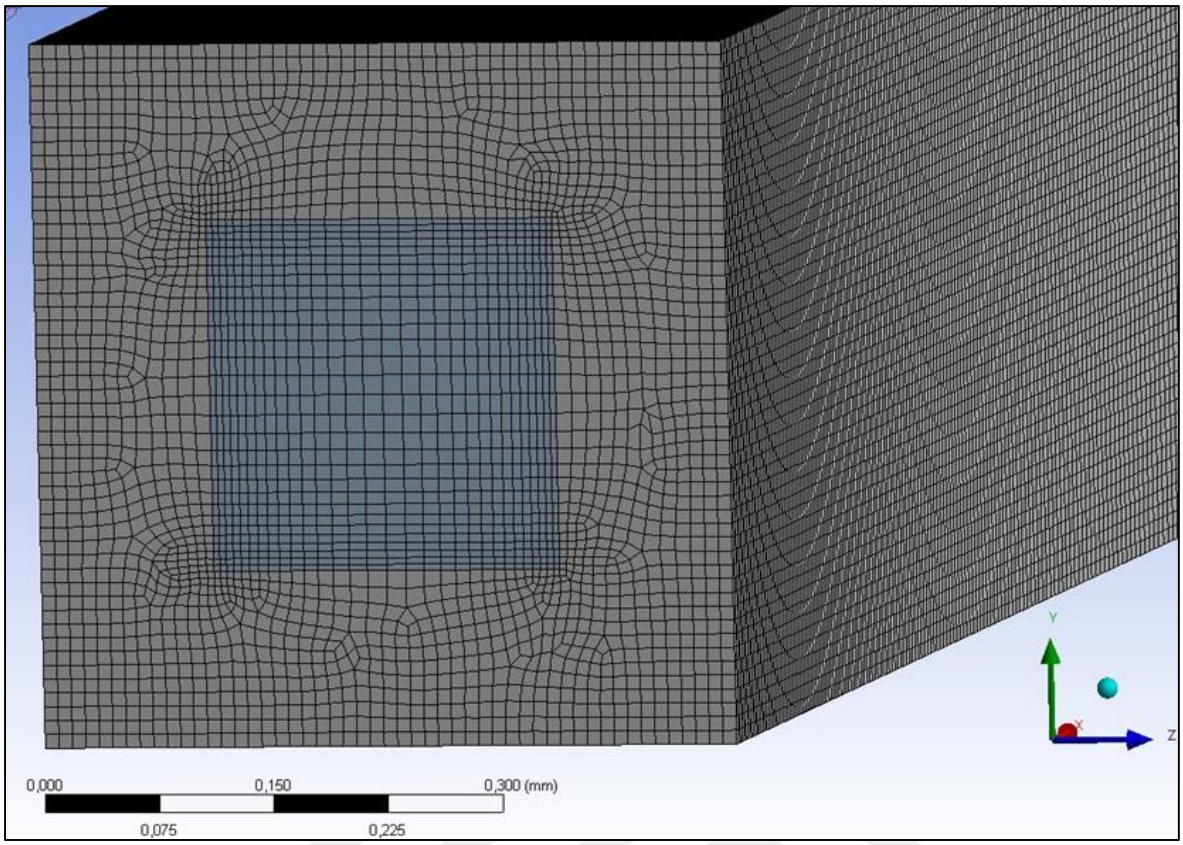

Figure A.3 : Solid region of Mesh_3 in M2_F3_AR1.

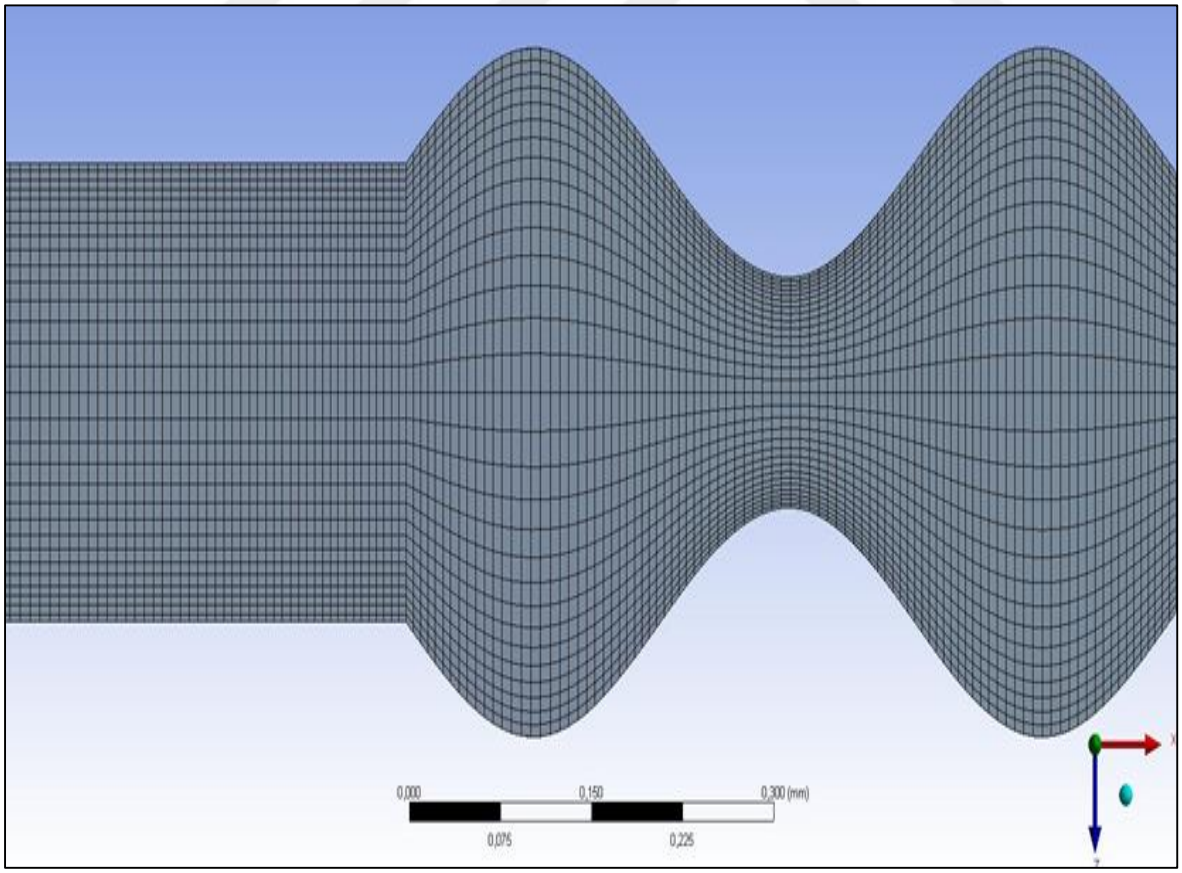

Figure A.4 : Fluid region of Mesh_3 in M2_F3_AR1.

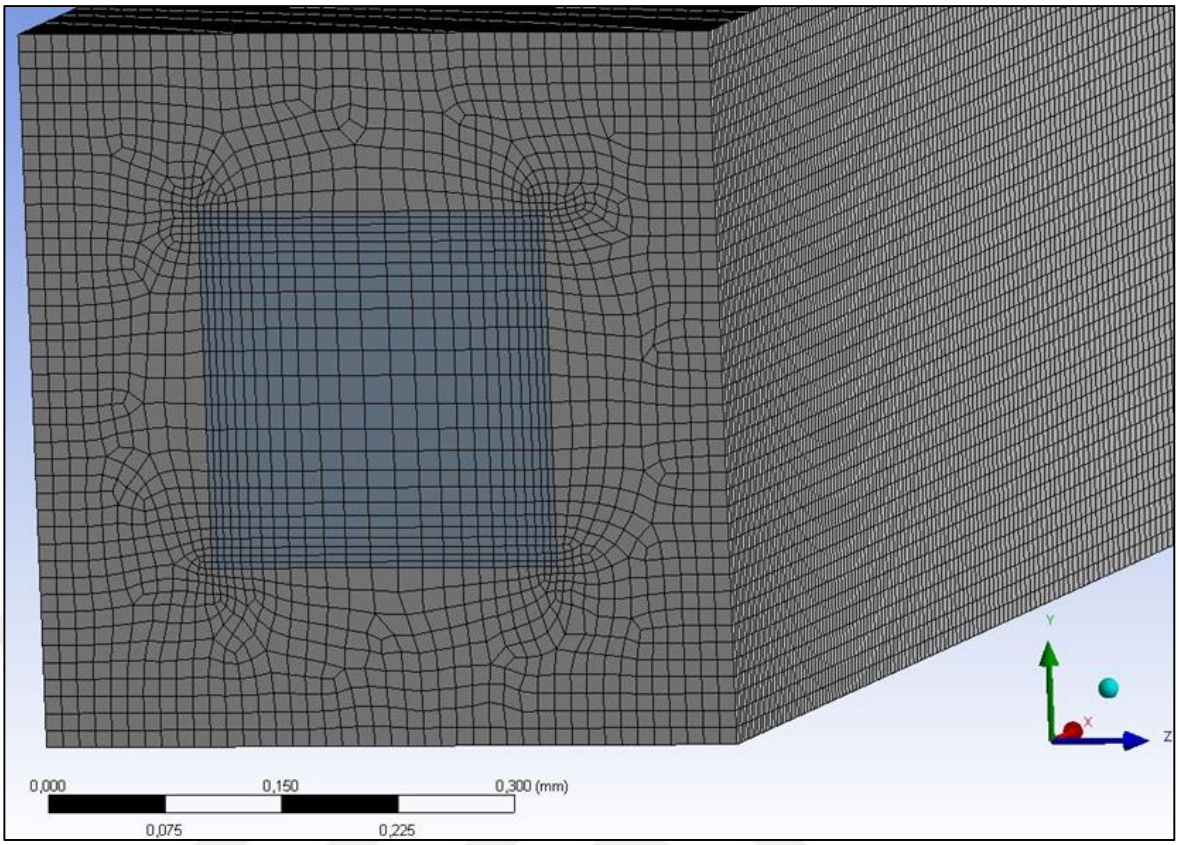

Figure A.5 : Solid region of Mesh_4 in M2_F3_AR1.

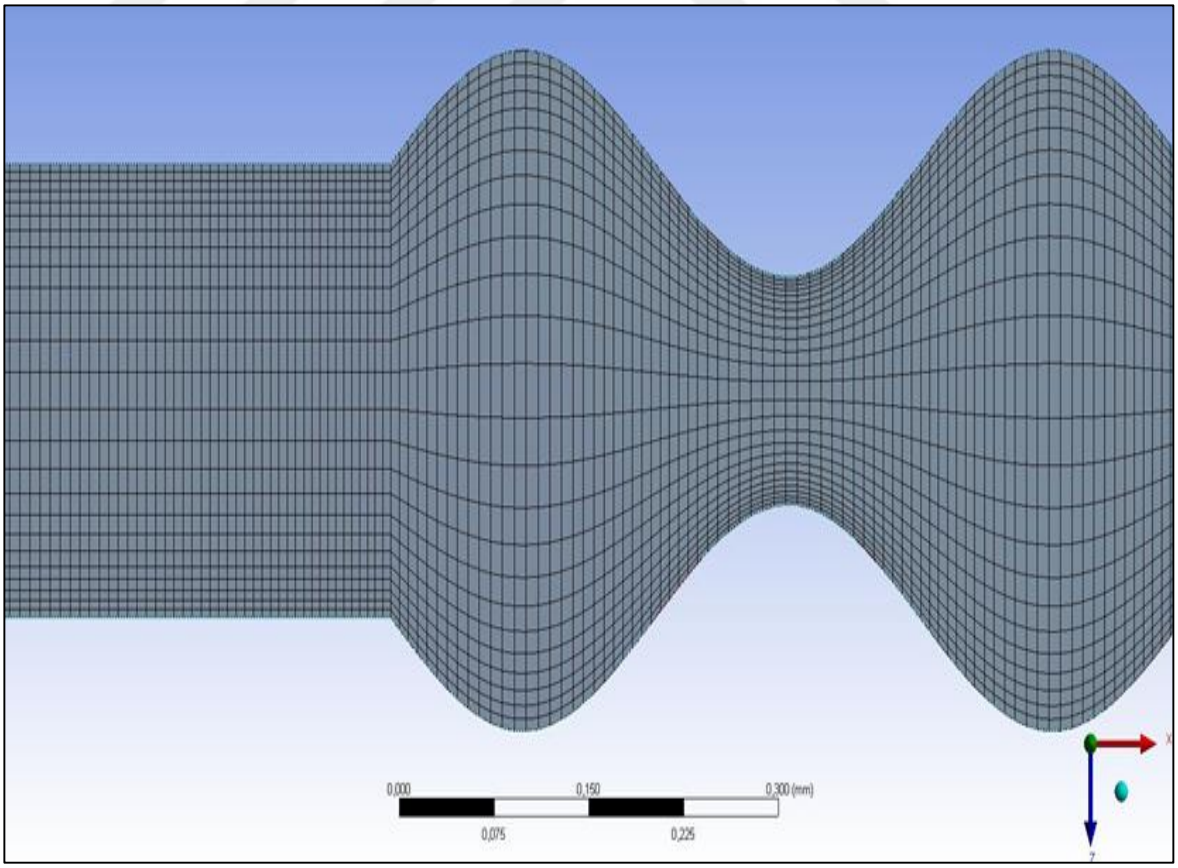

Figure A.6 : Fluid region of Mesh_4 in M2_F3_AR1.

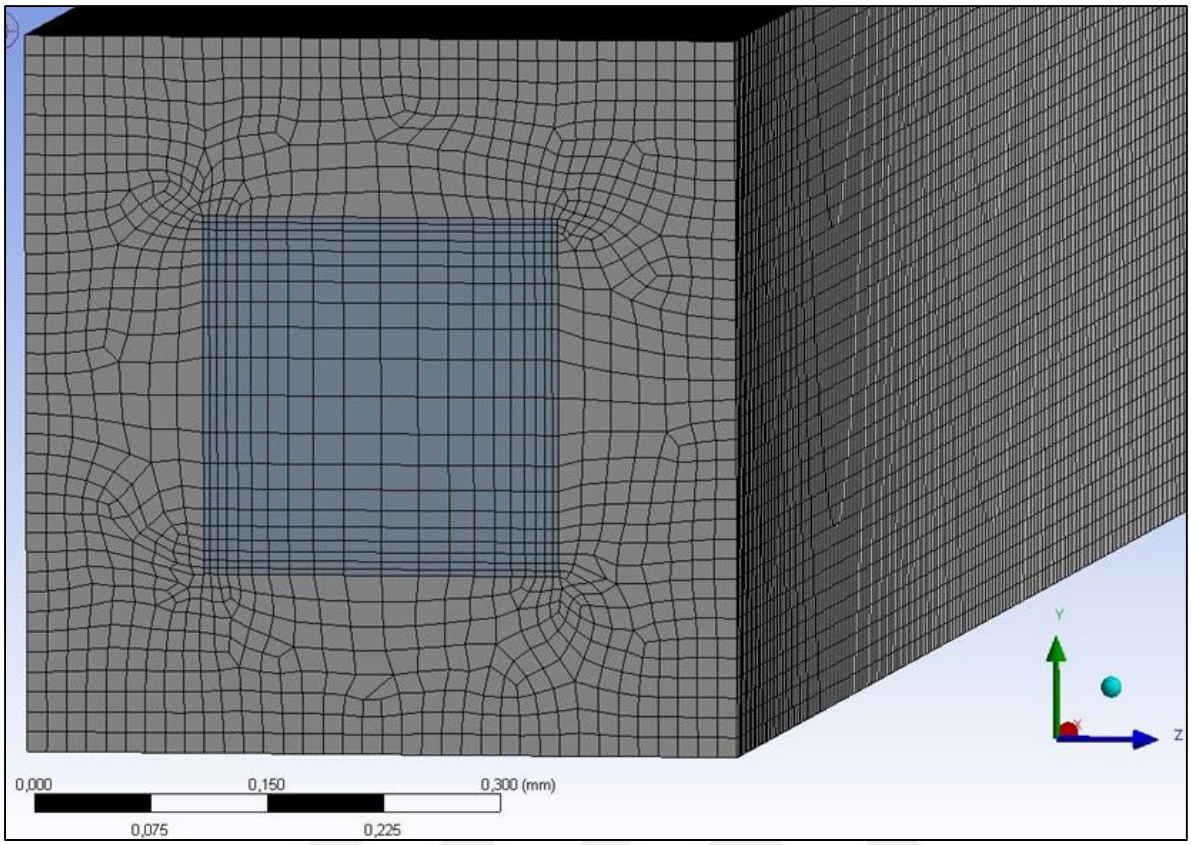

Figure A.7 : Solid region of Mesh_5 in M2_F3_AR1.

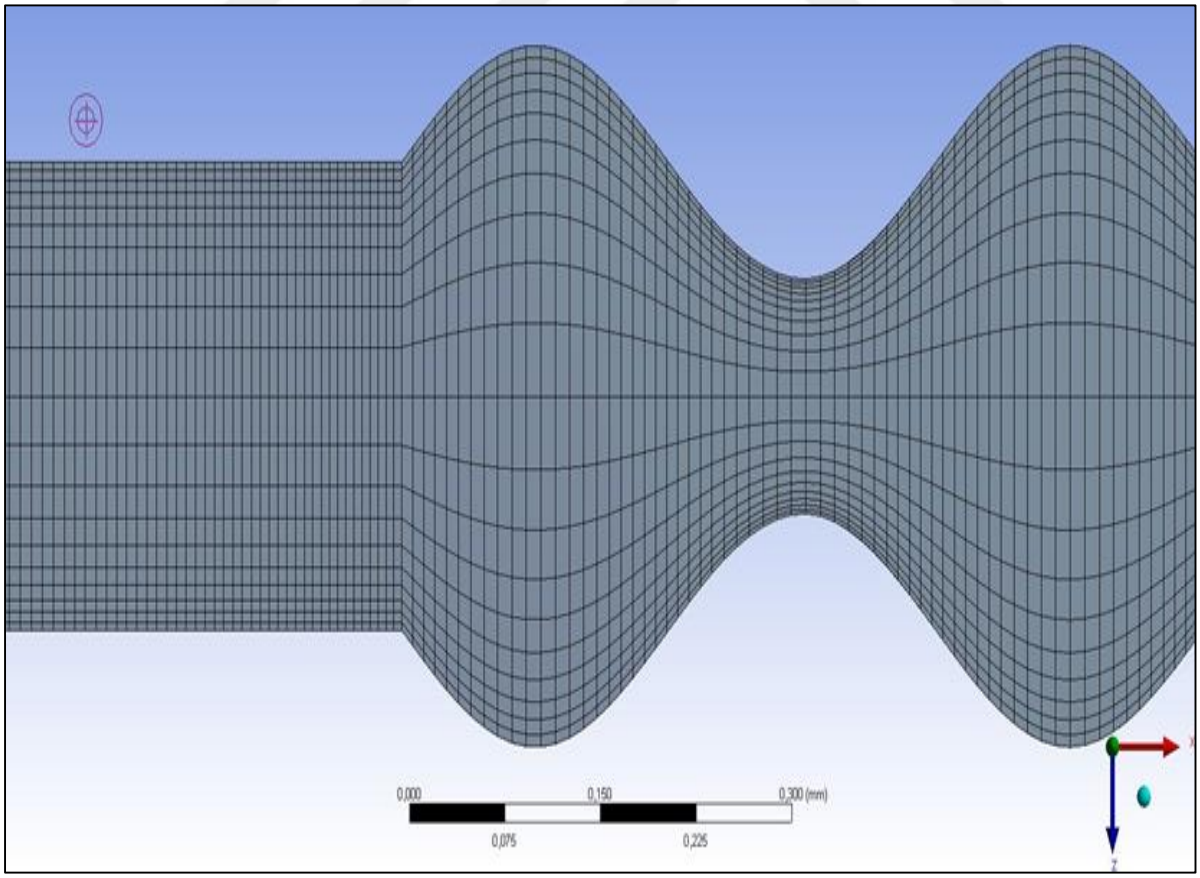

Figure A.8 : Fluid region of Mesh_4 in M2_F3_AR1.

APPENDIX B

```
#include "udf.h"

DEFINE_PROPERTY(cell_viscosity, cell, thread)
{
        real a_1;
        real a_2;
        real a_3;
        real a_4;
        real a_5;
        real x;
        real mu_lam;
        real temp = C_T(cell, thread);

        a_1 = (293.15 - temp) / (temp - 183.15);
        a_2 = 0.001303 * (293.15 - temp);
        a_3 = 0.00000306 * (293.15 - temp) * (293.15 - temp);
        a_4 = 0.0000000255 * (293.15 - temp) * (293.15 - temp) * (293.15 - temp);
        a_5 = a_1 * (1.2378 - a_2 + a_3 + a_4);
        x = pow(10, a_5);
        mu_lam = 0.001002 * x;

        return mu_lam;
}
```

CURRICULUM VITAE

Name Surname: Doğukan Arslan

E-Mail: arslandogukanitu@gmail.com

EDUCATION:

B.Sc.: 2015, Mechanical Engineering, Istanbul Technical University

PROFESSIONAL EXPERIENCE AND REWARDS:

Research Assistant in Gebze Technical University (2017 – in progress)